

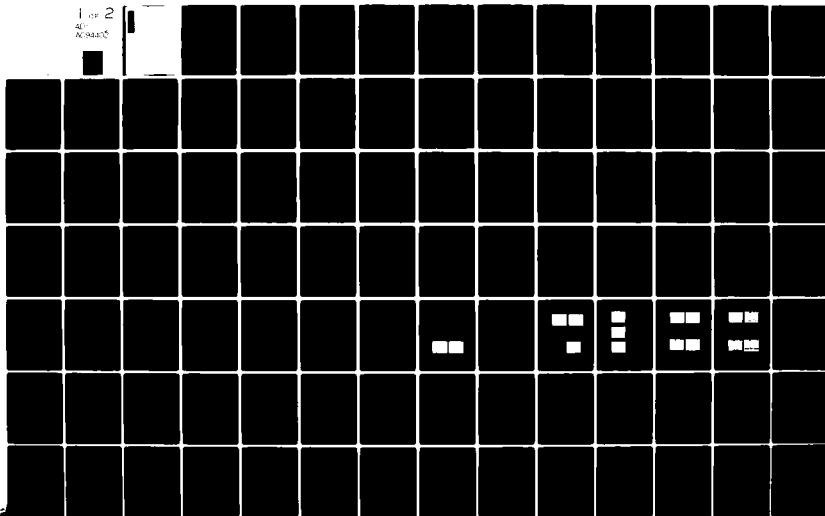
AD-A094 402

AIR FORCE INST OF TECH WRIGHT-PATTERSON AFB OH SCH00--ETC F/G 20/12
MEASUREMENT OF THE MINORITY CARRIER DIFFUSION RATE IN N-8AAS.(U)
DEC 80 G A BLEEKER
AFIT/6EO/PH/80-4

UNCLASSIFIED

NL

1 OF 2
AD-A094 402



AFIT/GEO/PH/80-4

LEVEL II

①

14 JAN 1981

APPROVED FOR PUBLIC RELEASE AFR 190-17.

Fredric C. Lynch
FREDRIC C. LYNCH, Major, USAF
Director of Public Affairs
Air Force Institute of Technology (ATC)
Wright-Patterson AFB, OH 45433

MEASUREMENT OF THE MINORITY
CARRIER DIFFUSION RATE IN
N-GaAs

THESIS

AFIT/GEO/PH/80-4

Gary A. Blecker
Capt USAF

Approved for public release; distribution unlimited

MEASUREMENT OF THE MINORITY
CARRIER DIFFUSION RATE IN
N-GaAs

THESIS

Presented to the Faculty of the School of Engineering
of the Air Force Institute of Technology
Air University

in Partial Fulfillment of the
Requirements for the Degree of
Master of Science

by

Gary A. Bleeker, B.S.E.E.

Capt USAF

Graduate Electro-Optics

December 1980

Accession For	
1	<input checked="checked" type="checkbox"/>
2	<input type="checkbox"/>
3	<input type="checkbox"/>
Dist	
Special	
A	

Approved for public release; distribution unlimited

Preface

The purpose of this thesis was to directly measure the diffusion rate of minority carriers in n-GaAs. This experiment was an original effort never before attempted. Due to the fact that the diffusion rates for reasonable sample thicknesses are in the sub-nano-second region, which is the limit of the equipment response, it was only possible to obtain an upper limit to the diffusion rate, a valid result, nevertheless.

Several interesting byproducts of the investigation were discovered and are discussed within this thesis.

I would like to thank my advisors, Paul Schreiber, from the Aero-Propulsion Laboratory, and Dr. Won Roh, from the AFIT faculty, who gave timely assistance, expert advice, and played the necessary role of devil's advocate.

Special acknowledgement is made of Don Reynolds, Senior Scientist for Electronic Technology, Avionics Laboratory, who provided insights into the physics of solid state materials; and to Sig Kizurnis of the Aero-Propulsion Laboratory who assisted during the actual conduct of the experiment.

Gary A. Bleeker

Table of Contents

Preface	ii
List of Figures	v
List Of Tables	viii
Abstract	ix
I. Introduction	1
Background	1
Problem and Scope	2
General Approach	2
Sequence of Presentation	3
II. Theoretical Basis of Experiment	4
General Model	4
Absorption	5
Exciton Formation	7
Diffusion	10
III. Equipment	19
Laser Excitation	19
Low Temperature Dewar	21
Filter/Spectrometer System	21
Detection System	22
Display System	23
IV. Procedure	25
Delay Measurement	25
Narrow Spectrum Delay Measurement	29
Spectroscopic Scan	31
Conversion Efficiency Measurement	33
V. Experimental Results/Discussion	35
Diffusion Rate Determination	35

Contents

Spectroscopic Study	38
Conversion Efficiency	42
VI. Conclusions	44
VII. Recommendations	46
Bibliography	50
Appendix A: Experimental Data	51
Appendix B: Computer Plots of Diffusion Equation Solution	57
Appendix C: Filter/Spectrometer Calibration . . .	74
Appendix D: Scattering Experiment	82
Vita	85

List of Figures

<u>Figure</u>		<u>Page</u>
1	Sample Construction	5
2	Energy Diagram of Active Layer	6
3	Bound Exciton Diagram	8
4	Energy Level Diagram Buffer Region	9
5	Energy Level/Excitons	11
6	Boundary and Initial Conditions	13
7	Plot of Solution to Diffusion Equation ($D=50, L=4\mu m$)	18
8	Typical Laser Pulse	20
9	Delay Measurement Schematic	26
10	Typical Optical Path Delay Measurement Output	28
11	Illustration of Delay	29
12	Narrow Spectrum Delay Measure- ment Schematic	30
13	Spectroscopic Scan Experiment	32
14	Conversion Efficiency Measure- ment Schematic	33
15	Typical Experimental Result	36
16	Typical Broadening	38
17	Spectroscopic Spectrum	39
18	Higher-than-Band-Gap Radiation	40
19	Mode-locked Laser/ 2 Photon Detection System	47
20	Two Photon Process	48
A-1	Experiment Photograph	51

List of Figures

(Continued)

<u>Figure</u>		<u>Page</u>
A-2 to A-8	Experiment Photographs	53-56
B-1	Computer Program	60
B-2	Computer Plot (D=25, L=4um)	61
B-3	Computer Plot (D=50, L=4um)	62
B-4	Computer Plot (D=100, L=4um)	63
B-5	Computer Plot (D=200, L=4um)	64
B-6	Computer Plot (D=50, L=8um)	65
B-7	Computer Plot (D=100, L=8um)	66
B-8	Computer Plot (D=50, L=10um)	67
B-9	Computer Program	68
B-10	Computer Plot (D=50, L=4um)	69
B-11	Computer Plot (D=100, L=4um)	70
B-12	Computer Plot (D=200, L=4um)	71
B-13	Computer Plot (D=50, L=8um)	72
B-14	Computer Plot (D=100, L=8um)	73
C-1	RG-715 Filter Response	74
C-2	Krypton Spectrum	76
C-3	Neon Spectrum	77
C-4	Intensity Profile of Standard Lamp	78
C-5	Spectrometer/Photomultiplier Calibration Set-up	79

List Of Figures
(Continued)

<u>Figure</u>		<u>Page</u>
C-6	ITT Photomultiplier Response	80
C-7	EMI Photomultiplier Response	80
C-8	Comparison of ITT/EMI Photo- multiplier Response	81
D-1	Scatter Experiment Schematic	82
D-2	Scatter Measurement Plot	84

List of Tables

<u>Table</u>		<u>Page</u>
I	Computer Data on Diffusion Equation Solution	59
II	Scatter Measurement Data	83

Abstract

A new experimental procedure was developed to directly measure the minority carrier diffusion rate in n-GaAs. A Q-switched Nd-YAG laser was used to excite the sample and the delay between laser excitation and subsequent luminescence of the sample was used to determine the diffusion rate.

A mathematical model of carrier diffusion was developed and computer plots generated to predict and analyze the experimental data. With the 4 micron thick sample used, the procedure enabled the researcher to obtain an upper bound in delay time of 350 picoseconds and an approximate diffusion coefficient of $100 \text{ cm}^2/\text{sec}$.

The spectral components of the luminescence and relative conversion efficiency were studied. The luminescent spectra exhibited yet unidentified lines above the band gap energy in addition to the usual set of exciton lines. The conversion efficiency of the laser excitation to photoluminescence was 0.14%.

Introduction

Background

The quality of the active layer in semiconductor devices such as field-effect transistors (FET) and high speed logic circuits plays a crucial part in determining overall performance characteristics of the devices. The quality of the active layer can be evaluated by measuring device parameters such as mobility and the diffusion rate. Despite this need, the diffusion rate of holes in n-GaAs has never been measured.

The forerunner of experiments of this type is the famous Haynes-Shockley experiment which was the first successful direct measurement of carrier drift velocity. (Ref 1:342). Although measurement of drift velocity is not the purpose of this thesis, some of the experimental techniques are applied to this experiment. Few relevant experiments have been performed with GaAs in the low temperature regime. Of particular importance were spectroscopic experiments by Don Reynolds of the Avionics Laboratory. (Ref 2) These experiments laid the basic theoretical foundation for performance of this experiment.

This thesis effort, sponsored by the Avionics and Aero-Propulsion Laboratories was an attempt to use a new experimental technique to make direct measurements of the diffusion rate of the minority carrier in n-GaAs.

Problem and Scope

The primary objective of this research project was to determine experimentally the diffusion rate of the minority carrier (holes) in n-type GaAs by a photoluminescent method. Various experimental techniques were developed to study diffusion rates in the sub-nanosecond time regime. Spectroscopic methods were utilized to isolate particular emission wavelengths of the photoluminescence. A theoretical model was developed using the standard ambipolar diffusion equation and computer generated plots were obtained.

General Approach

The basic experimental method is to generate a large number of hole-electron pairs at the surface of an active layer by the use of a short, intense laser pulse. The hole-electron pairs diffuse across the active layer and are forced to recombine at an interface region between the active layer and the buffer material. The recombination produces photons which are detected. The time difference between the initial laser pulse creating the hole-electron pair and the recombination radiation emitted at the interface is measured to determine the diffusion rate. The radiative lifetime of the exciton is assumed to be very short and can be neglected as a contribution to the delay.

Sequence of Presentation

The theoretical basis for the experiment is presented in Chapter II. Some computer plots of the solution to the diffusion equation will be presented at that time. In Appendix B, the computer program and a series of plots made using different parameters will be presented. The equipment used to perform the experiment will be described in Chapter III with calibration techniques and results of that calibration detailed in Appendix C. Chapter IV will present the experimental procedures. The results and discussion will appear in Chapter V. The conclusions will appear in Chapter VI and recommendations for further study in Chapter VII.

II. Theoretical Basis of Experiment

First presented is a general theoretical model used to develop and experiment for determining the minority carrier diffusion rate, then a discussion of the various processes involved and assumptions made.

General Model

The physical makeup of the sample is that of a moderately doped (10^{17}) n-type GaAs layer 4 microns thick on an intrinsic epitaxial buffer material. (See Figure 1) The sample was provided by the Avionics Laboratory.

A high energy, pulsed, Nd-YAG laser is used to create an instantaneous plane wave source of hole-electron pairs that diffuse across the active layer. There is no significant recombination of these free hole-electron pairs (the minority carriers in this case are holes) in the active region. These pairs are "forced" to recombine at the interface between the active and buffer regions. The recombination, primarily through the formation of various exciton, is seen as photoluminescence. The time taken by the minority carrier to diffuse is obtained by measuring the time difference between the initial laser pulse and the radiation produced at the interface. The radiative lifetime of the exciton is assumed to be short and neglected as a component of the delay.

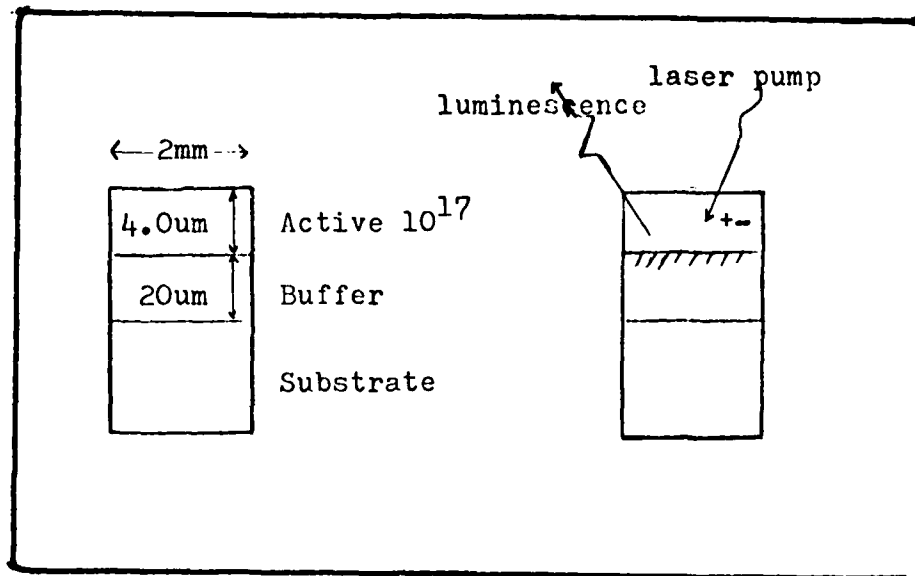


Figure 1. Sample Construction

Absorption

The incident laser pulse consists of 532 nanometer (556nm line also observed: See Appendix D) radiation with a spot size about the size of the sample width (2mm) but much bigger than the sample depth. The incident radiation can therefore be considered as a plane wave source. There are well documented (Ref 3:637) absorption coefficients (α) of approximately $5 \times 10^4 \text{ cm}^{-1}$ or larger at this wavelength. The absorption depth is consequently very small. Using Beer's Law

$$I(x) = I_i e^{-\alpha x} \quad (1)$$

where $I(x)$ = Intensity at depth x

I_i = Incident Intensity

One can show that the incident light is 87% absorbed within

0.4 microns. The active layer is 4 microns thick in comparison. The incident photon density was calculated to be approximately 10^{21} photons/cm³. Since this is some orders of magnitude below the crystal density, it is safe to assume that there is no bleaching. It has been shown by Ettenberg (Ref 4:210) that reabsorbed recombination radiation can be neglected. His experimental evidence showed that the carriers created by reabsorbed recombination radiation represented less than 10% of the total carriers diffusing from the generating source. The probability of recombination within the active region is extremely low. Doping at the 10^{17} cm⁻³ level results in a Fermi level 12 meV above the conduction band edge. In the case under discussion, known as degenerate, the Fermi level is indeed within the conduction band. Figure 2 illustrates this using an energy level diagram.

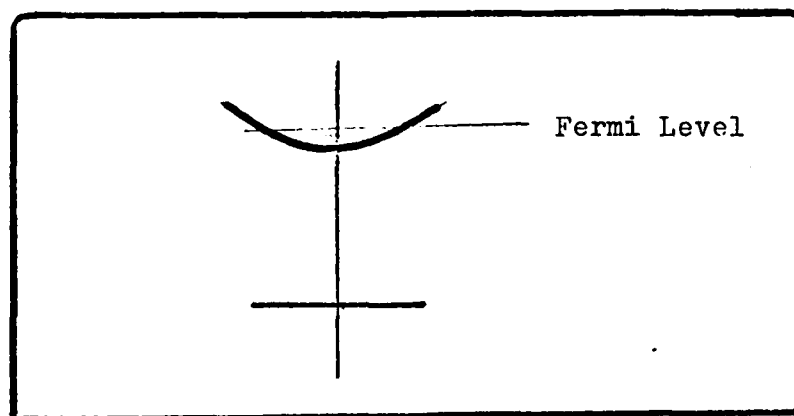


Figure 2. Energy Diagram of active Layer

There are so many free electrons and the impurities

are in such close proximity that the energy levels are essentially a continuum, very similiar to the banding of energy levels which takes place in metals. These free electrons are free to diffuse across the active layer.

Exciton Formation

Excitons can be thought of in terms of two limiting approximation, one due to Frenkel, in which the exciton is considered tightly bound and a later approximation due to Mott and Wannier where the exciton is weakly bound having an electron-hole interparticle distance larger than an atomic radius. The weakly bound state (commonly known as a free exciton) can be considered as the union of a hole and electron whose combined energy is just below the energy of the conduction band. The formation is much like that of a hydrogen aton with energy levels described by a modified Rydberg equation. (Ref 5:504-505). A bound exciton occurs when an electron-hole pair orbits around an impurity atom. This is illustated diagrammatically in Figure 3. The pair can be attached to either a donor or an acceptor atom. However, the binding energy of the donor bound exciton is 1 meV, while the acceptor bound exciton binding energy is 3 meV. The emission of radiation during the exciton decay process is known as luminescence and is the source of the emitted

light used in this experiment.

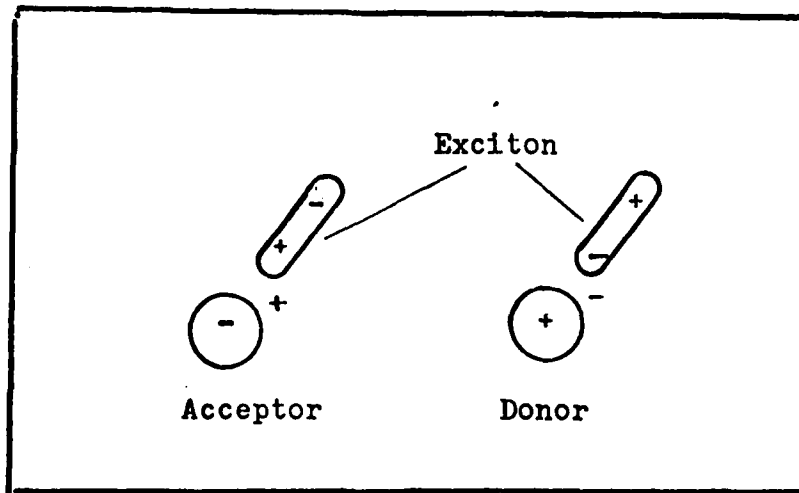


Figure 3. Bound Exciton Diagram

In this experiment, the hole-electron pairs diffuse across the active region until they encounter the active-buffer interface. The buffer is intrinsic (compensated) and contains equal numbers of donors and acceptors at 10^{14} cm^{-3} . In comparison to the doping level of the active layer, these impurity atoms can hardly "see" each other. As a consequence, the energy levels are now discrete in nature and the hole-electron pairs are forced to recombine by exciton formation. Direct recombination between free electrons in the conduction band and a free hole in the valence band is highly unlikely. However, a number of lower than bandgap energy exciton states are available. The reader should refer to Figure 4 for the following discussion.

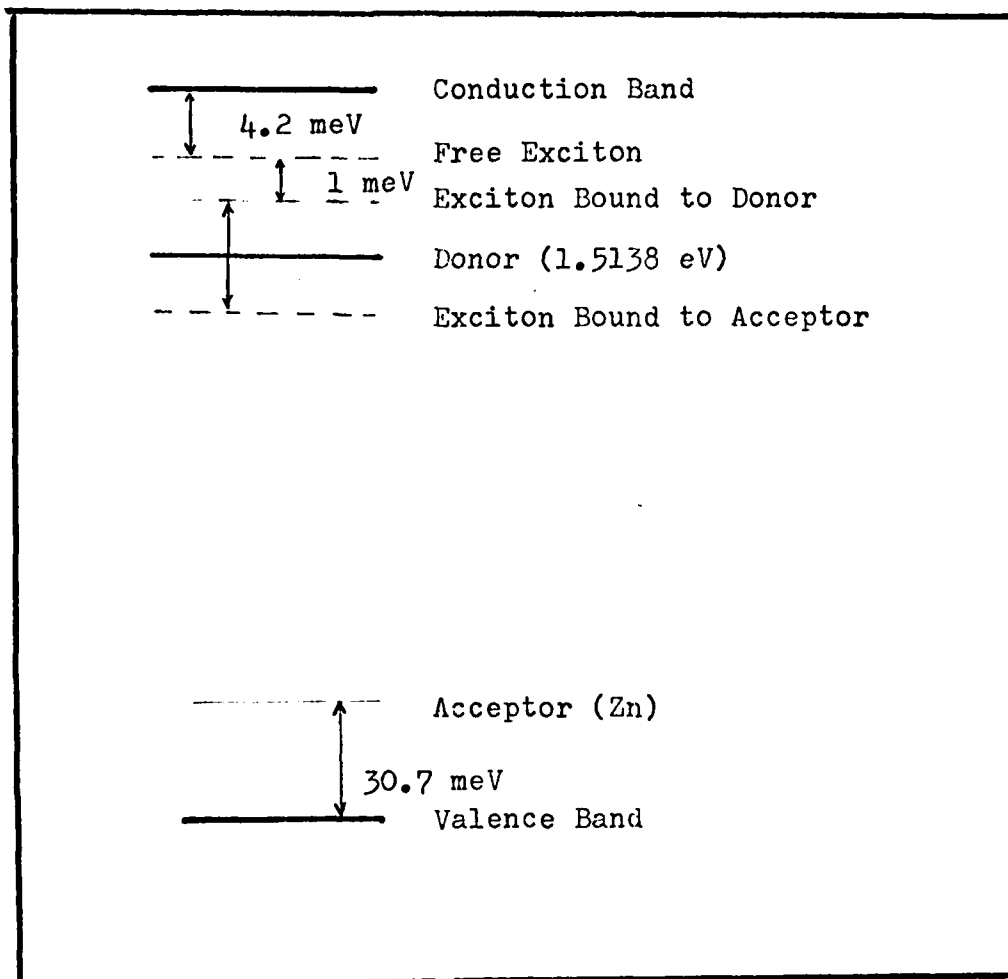


Figure 4. Energy Level Diagram-Buffer Region

Free excitons can be formed at an energy level 4.2 meV lower than the band gap. Liquid helium temperatures are required for viewing excitons because higher temperatures squelch their formation due to the low binding energies involved. Excitons bound to donors can be formed 1 meV lower than the free exciton, this energy being due to the binding energy of the exciton bound to a donor. Approximately 3 meV below the energy level of the bound donor

state is the exciton bound to an acceptor. Other possible, but not as probable recombinations include a free electron in the conduction band with an acceptor, and a bound donor to bound acceptor transition. Phonon replicas differing by 36.4 meV in energy are also possible. Figure 5 (on the next page) illustrates the indicated energy levels and their associated energy and wavelength. All recombination mechanisms discussed occur at the interface region and are therefore useful as a means to measure the diffusion rate.

Diffusion

Diffusion is the transport of particles within a material due to the presence of concentration gradients. The diffusion in semiconductors is typically denoted by the ambipolar diffusion equation which is an extension of Fricke's law. A useful form of the equation follows Ref 1:327):

$$\frac{D\delta^2 p}{\delta x^2} - \mu \frac{E\delta p}{\delta x} - \frac{p}{t_p} = \frac{\delta p}{\delta t} \quad (2)$$

where

D is the diffusion coefficient
 μ is the mobility
 E is the applied electric field
 t_p is the recombination time constant
 p is the particle concentration of holes

The second and third terms of the equation are eliminated in this treatment because there is no external applied

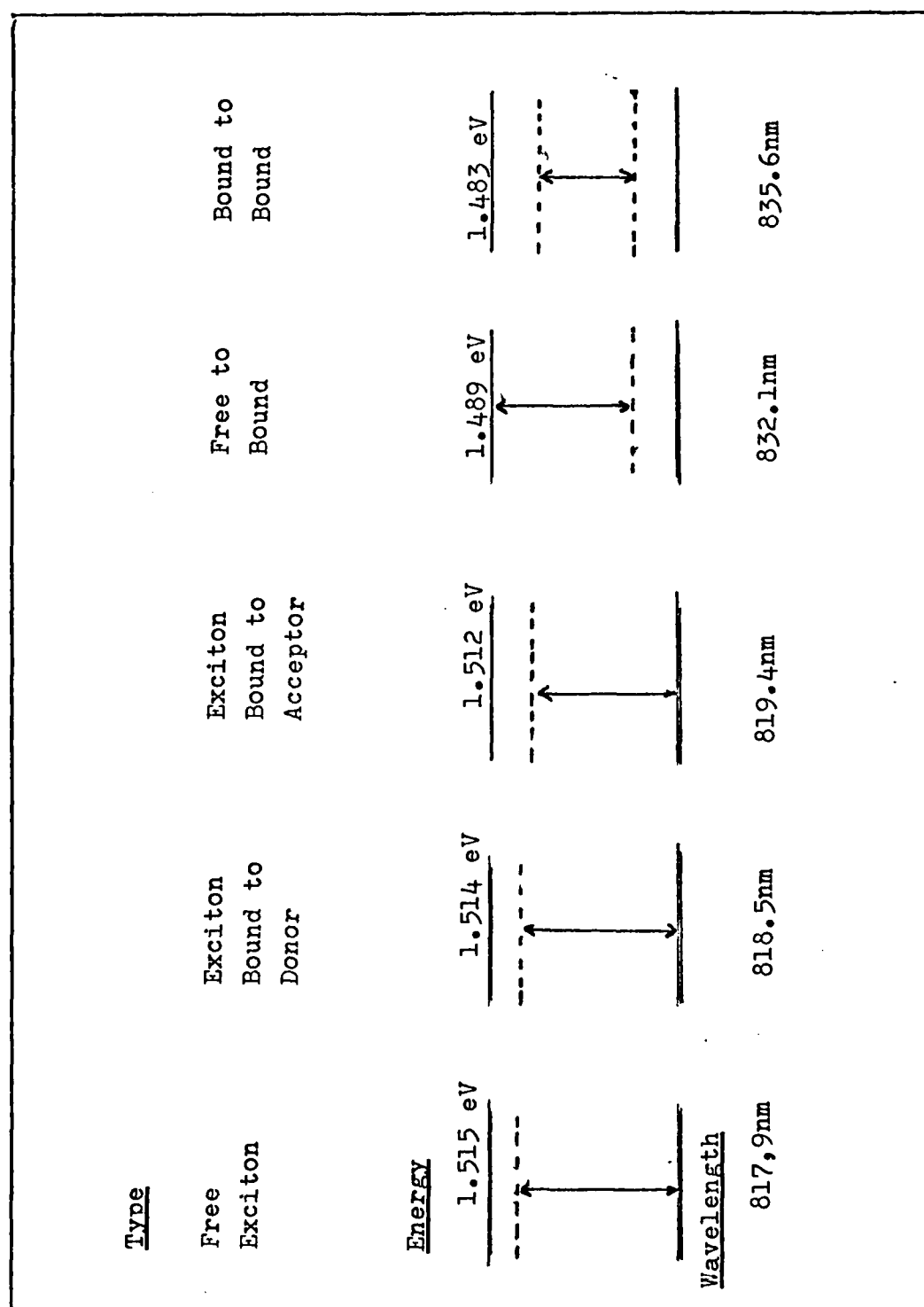


Figure 5. Energy Levels/Excitons

field and little recombination within the active layer occurs. This results in the following simplified equation.

$$D \frac{\delta^2 p}{\delta x^2} = \frac{\delta p}{\delta t} \quad (3)$$

The following is a development of a solution to the diffusion equation. Equation (3) can be solved using Laplace Transform techniques where both sides of Eq (3) are multiplied by e^{-st} and integrated with respect to time from 0 to ∞ .

$$\int_0^{\infty} e^{-st} \left[\frac{\delta^2 p}{\delta x^2} \right] dt - \frac{1}{D} \int_0^{\infty} e^{-st} \left[\frac{\delta p}{\delta t} \right] dt = 0 \quad (4)$$

Letting $v(s)$ be the Laplace Transform of $P(x,t)$

$$v(s) = \int_0^{\infty} e^{-st} p(x,t) dt \quad (5)$$

interchanging the order of differentiation and integration yields

$$\frac{\delta^2 v(s)}{\delta x^2} - \frac{s}{D} v(s) = 0 \quad (6)$$

The second term of Eq (6) is obtained by integration by parts of the second term of Eq (4) after applying the initial condition ($t=0, P=0$). The solution to Eq (6) is

$$v(s) = A_1 e^{-\sqrt{s/D} x} + A_2 e^{\sqrt{s/D} x} \quad (7)$$

The experiment can be represented by a source-sink

model with a source at the absorption edge and a sink at the active-buffer layer interface. The boundary and initial conditions are illustrated in Figure 6. $I_i(t)$ is the incident intensity, α is a constant, and J is the internal particle current.

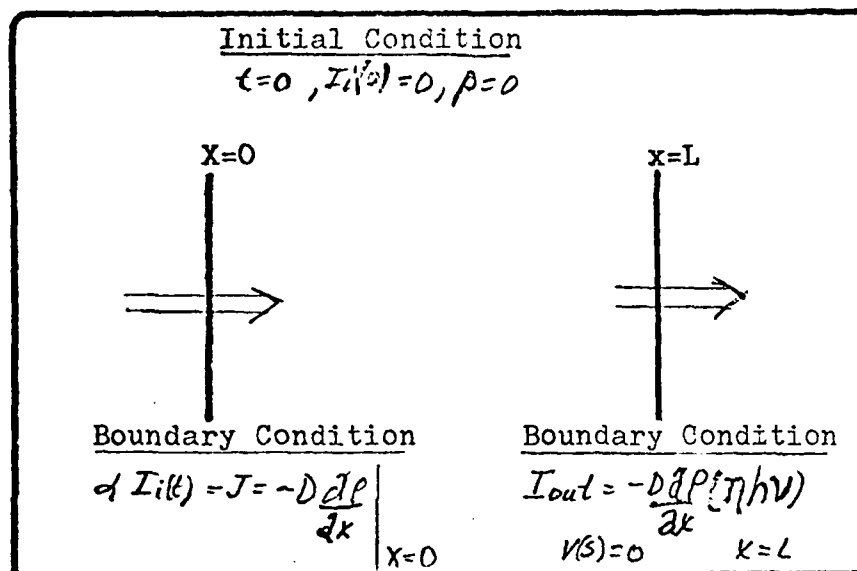


Figure 6. Boundary and Initial Conditions

differentiating both sides of Eq (5) and multiplying by D yields

$$\frac{D \delta v(s)}{\delta x} = \int_0^{\infty} D \frac{\delta P(x,t)}{\delta x} e^{-st} dt \quad (8)$$

but

$$-\int_0^{\infty} D \frac{\delta P(x,t)}{\delta x} \Big|_{x=0} e^{-st} dt = \alpha \int_0^{\infty} I_i(t) e^{-st} dt \quad (9)$$

Taking Eq (7) and differentiating with respect to x yields

$$\frac{\delta v(s)}{\delta x} = -A_1 \sqrt{s/D} e^{-\sqrt{s/D} x} + A_2 \sqrt{s/D} e^{+\sqrt{s/D} x} \quad (10)$$

but
$$\left. \frac{\delta V(s)}{\delta x} \right|_{x=0} = -\frac{\alpha}{D} \int_0^{\infty} I_i(t) e^{-st} dt \quad (11)$$

from Eqs(8) and (9). Then letting

$$\sqrt{s/D} = q \quad (12)$$

results in

$$-\frac{\alpha}{D} \int_0^{\infty} I_i(t) e^{-st} dt = \left[-A_1 q + A_2 q \right] \Big|_{x=0} \quad (13)$$

Therefore

$$A_1 - A_2 = \frac{\alpha}{qD} \int_0^{\infty} I_i(t) e^{-st} dt \quad (14)$$

The boundary condition at the active-buffer interface

is $v(s) = 0$ at $x=L$. From Eq (7)

$$-A_1 e^{-qL} = A_2 e^{+qL} \quad (15)$$

$$A_2 = -A_1 e^{-2qL} \quad (16)$$

Therefore

$$A_1 (1 + e^{-2qL}) = \frac{\alpha}{qD} \int_0^{\infty} I_i(t) e^{-st} dt \quad (17)$$

So

$$A_1 = \frac{\alpha \int_0^{\infty} I_i(t) e^{-st} dt}{qD (1 + e^{-2qL})} \quad (18)$$

The total equation is now (Form of Eq (7))

$$v(s) = \frac{\alpha/qD \int_0^{\infty} I_i(t) e^{-st} dt (e^{-qx} - e^{qx-2qL})}{(1 + e^{-2qL})} \quad (19)$$

The goal of this development is to find I_{out} , that is, the radiation that is measurable with a photodetector. The output is given by

$$I_{out} = -D \frac{\delta \rho}{\delta x} \eta h \nu \Big]_{x=L} \quad (20)$$

where η = Efficiency
 h = Planck's Constant
 ν = Frequency

And from Eq (8) at the boundary $x=L$

$$-D \frac{\delta v(s)}{\delta x} \Big|_{x=L} = - \int_0^{\infty} \frac{\delta \rho}{\delta x} \Big|_{x=L} e^{-st} dt \quad (21)$$

differentiating Eq (19) with respect to x

$$-D \frac{\delta v(s)}{\delta x} = -\alpha \frac{(e^{-qx} + e^{-2qL} e^{2x})}{(1 + e^{-2qL})} \int_0^{\infty} I_i(t) e^{-st} dt \quad (22)$$

and solving for $x=L$, then taking the inverse Laplace transform of both sides results in

$$I_{out} = \mathcal{L}^{-1} \left[\beta \left[\int_0^{\infty} I_i(t) e^{-st} dt \right] \left[\frac{2 e^{-qL}}{(1 + e^{-2qL})} \right] \right] \quad (23)$$

where \mathcal{L}^{-1} is the inverse Laplace Transform and β is a constant equal to $\eta h \nu$. Now $1/(1 + e^{-qL})$ can be represented by the series expansion.

$$\frac{1}{1+\tau} = 1 - \tau + \tau^2 - \tau^3 + \tau^4 - \dots \quad (24)$$

where $\tau = e^{-2qL}$

Therefore Eq (23) can be simplified to

$$I_{out} = \mathcal{L}^{-1} \left[2\beta \left[\int_0^{\infty} I_i(t) e^{-st} dt \right] \left[e^{-qL} - e^{-3qL} + e^{-5qL} - \dots \right] \right] \quad (25)$$

The second and higher order terms correspond physically to reflections from the interface. They will be considered negligible in this treatment.

If the input $I_i(t)$ is represented by a dirac delta $\delta(t)$ function, the first term in the expression is the Laplace transform of a delta function which is a constant

$$\int_0^{\infty} I_0 \delta(t) e^{-st} dt = I_0 \quad (26)$$

The output reduces to the inverse Laplace Transform of e^{-qL} with a constant multiplier.

$$I_{out} = I_0 \alpha 2\beta \int_0^{-1} [e^{-qL}] \quad (27)$$

Use of transform tables (Ref 6:377) developed for diffusion problems yields

$$I_{out} = \alpha \beta I_0 \left[\frac{x}{\sqrt{\pi D t^3}} e^{-\frac{x^2}{4Dt}} \right] \quad (28)$$

where $\beta = nh\nu$

Another candidate function which more accurately represents the laser pulse input is that of a rectangular function whose width is that of the laser input pulse (Approximately 500 picoseconds). Taking the Laplace Transform of a rectangular pulse (that is what the expression in the first bracket in Eq (25) denotes) is as follows;

$$\int_{t_0}^{t_1} 1 e^{-st} dt = \frac{e^{-st_1} - e^{-st_0}}{-s} \quad (29)$$

A reasonable t_0 would be zero, so Eq (29) reduces to

$$\frac{1 - e^{-st_1}}{s} = \mathcal{L}^{-1} [R_{ECT}] \quad (30)$$

Rewriting Eq (25) yields

$$I_{OVT} = 2\alpha\beta \mathcal{L}^{-1} \left[\left[1 - e^{-st_1} \right] \left[\frac{e^{-qL}}{s} \right] \right] \quad (31)$$

From Laplace Transform theory it is known that $e^{-bs} F(s)$ transforms into $F(t-b) u(t-b)$, where $u(t-b)$ is a unit step function at $t=b$. Now the transform of e^{-qL}/s is $ERFC(x/2\sqrt{Dt})$ (Ref 6:377). So the total solution can be written as

$$I_{OVT} = 2\alpha\beta \left[ERFC\left(\frac{x}{2\sqrt{Dt}}\right) - ERFC\left(\frac{x}{2\sqrt{D(t-t_1)}}\right) u(t-t_1) \right] \quad (32)$$

Both Equations (28) and (32) were plotted by computer for various values of diffusion constant D and sample thicknesses L . These are contained in Appendix B. A typical example for $D=50 \text{ cm}^2/\text{sec}$ and $L=4 \text{ microns}$ is shown in Figure 7. These plots were used by the experimenter to analyse the data.

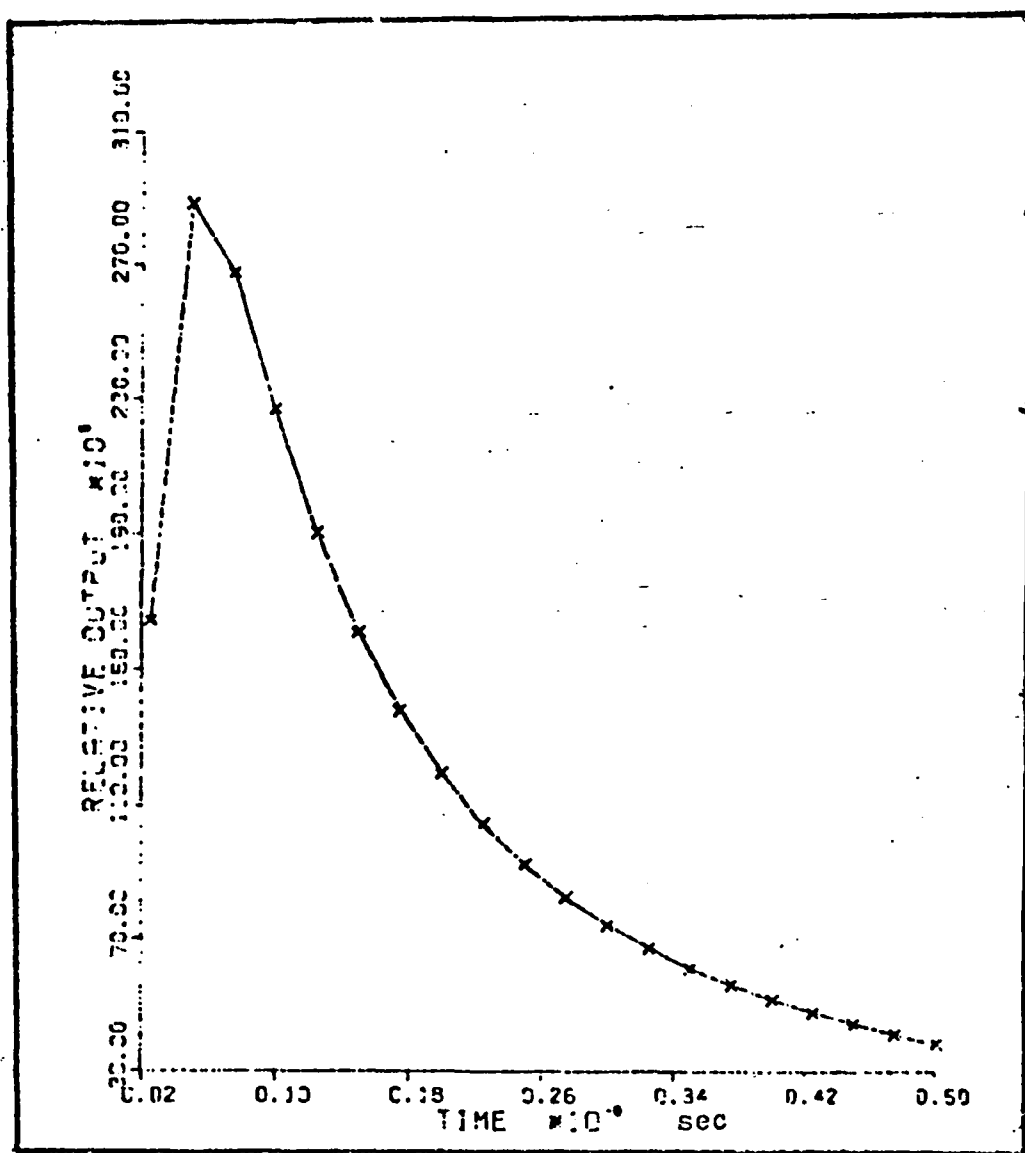


Figure 7. Plot of Solution to Diffusion Equation
($D=50, L=4\mu m$)

III. Equipment

The equipment used in the experiment can be divided into five main categories. These include 1) The laser excitation source, 2) The low temperature dewar, 3) Filter/Spectrometer system, 4) Detection system, and 5) Display system.

The laser output is directed onto the sample located in a low temperature dewar. The radiation emitted by the sample is collected and filtered before entering the photodetection system. The output of the photodetector is then coupled to an oscilloscope or a chart recorder for display. A small portion of the primary beam is used to provide a reference signal. Specific experimental set-ups will be described in Chapter IV (Experimental Procedure).

Laser Excitation

A GTE/Sylvania Model 618 Q-switched Nd:YAG laser was used as the primary excitation source. The laser emits light at 1.064 microns. The output was then doubled by a standard KDP crystal doubler to provide 532 nanometer radiation. The doubled output was filtered by two 1.06 micron blocking filters to remove all possible vestiges of 1.06 micron radiation. The laser was repetitively pulsed at 25 pulses/sec. A typical laser pulse is shown in Figure 8.

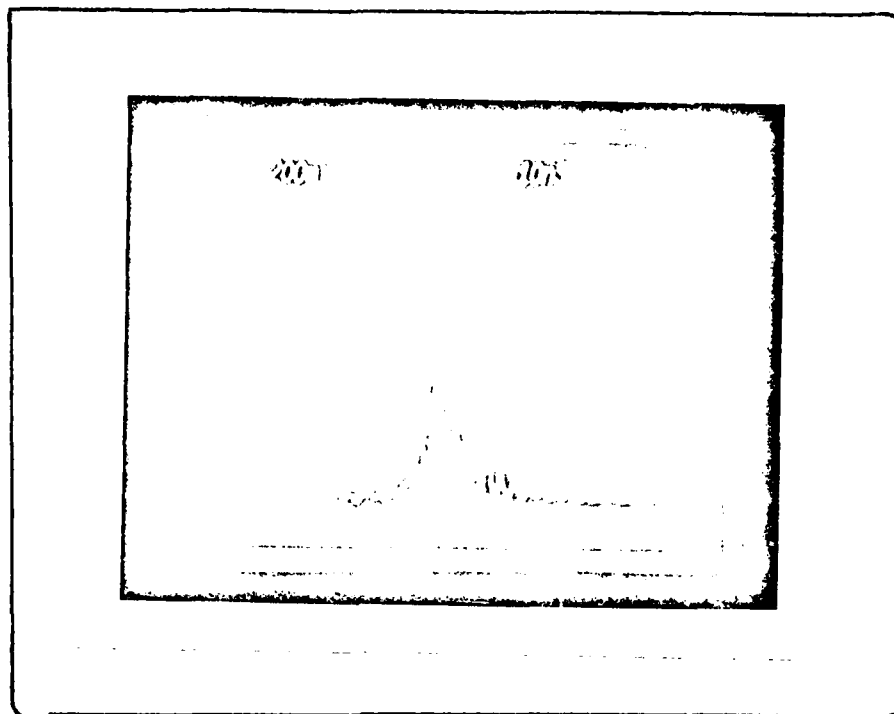


Figure 8. Typical Laser Pulse

One can see that it is actually composed of numerous short (less than 1 nanosecond) pulses. These pulses are actually the temporal representation of interference created by the various frequency domain components under the laser gain curve. This mode locked pulse train is generally not visible with standard laboratory detectors and oscilloscopes. A typical representation of a Q-switched laser pulse is a smooth gaussian shape. These short pulses were used to advantage by the experimenter to provide excitation pulses of very short duration. For some experimental procedures, a red saturable dye (Rhodamine 6 G) was used to select only the higher peak pulses in the pulse train. This enabled the researcher to consistently produce less than 1 nanosecond pulses.

Low Temperature Dewar

The sample was mounted with rubber cement on a metal rod totally immersed in the inner jacket of a low temperature dewar. The dewar consisted of an outer vacuum jacket, an inner nitrogen jacket and a 2 liter internal helium reservoir. After filling, the helium was pumped using a vacuum pump to bring the helium below the laminar flow point. Pumping below the laminar flow point insured cooling down to 2°K. The dewar contained high clarity transmission windows located at 90° increments permitting virtually unobstructed access to the sample. The sample could be rotated by the use of the rod holder. Generally, the sample was oriented normal to the incoming laser excitation.

Filter/Spectrometer System

After the sample was illuminated by the source, the photoluminescent emission was collected by use of a short-focal length lens, then "filtered" by the use of an optical low pass filter or a spectrometer.

The optical low pass filter was a type RG-715 filter whose response curve is shown in Appendix C. Basically, it allows light of 750 nanometers or longer to pass unimpeded.

For more precise wavelength isolation and for spectroscopic scanning experiments, a small Jobin-Yvon

Spectrometer Model 5/392UV was used. This spectrometer was calibrated using a number of spectral lamps such as K, Ar, Ne, Rb, and Cs to insure accurate calibration. It was found to be accurate to within 0.5 nanometers. The spectral plots used for calibration are contained in Appendix C.

Detection System

The filtered emission was directly coupled into the detection system. An ITT F4000 vacuum photodiode whose rated response time is better than 500 picoseconds with a S-1 cathode was used. The RG-715 filter was taped directly to the photodiode mount to insure that no 532 nanometer radiation leaked through. The vacuum photodiode was biased at 1500 Vdc. The S-1 response curve is relatively flat in the 800-900 nanometer region.

For more precise filtering and for spectroscopic scanning, an ITT F4102 photomultiplier was mounted by use of a light-tight coupling to the spectrometer. The F4102 photomultiplier was rated at 500 picosecond response time and used an S-20 cathode material. The actual response time appeared to be 1 nanosecond or more. The RG-715 filter was also placed in front of the spectrometer to eliminate all possibility of leakage of the 532 nanometer laser beam. A 1 RPM motor drive was connected to the spectrometer for scanning experiments and the photomultiplier was biased by a 4000 Vdc power supply. A total

calibration of the filter, spectrometer, and photomultiplier combination response was performed using a standard lamp and is shown in Appendix C.

An EMI Type 9816 photomultiplier was also used in place of the ITT F4102 to verify results. Calibration is also shown in Appendix C.

A hole was drilled into the coupling between the spectrometer and the photomultiplier to allow insertion of a fiber-optic cable. This fiber-optic link was necessary to permit a reference signal to impinge upon the photomultiplier for some experiments.

In addition to the fast detectors mentioned, a Scientech 362 Power/Energy meter was used to measure the 532 nanometer beam power for the conversion efficiency experiment.

Display System

The output of the photodetectors is coupled to the input of an oscilloscope or chart recorder by use of a short 50 ohm coaxial cable

The oscilloscope used was a Tektronix 7104 mainframe which contained either a 7A29 or 7A19 vertical amplifier. The 7A19 is good to 600 MHz and the 7A29 to 1.2 GHz. Both inputs are 50 ohm for fast response. The 7A29 is capable of 350 picosecond rise time, however it was unavailable

for part of the experiment. Precision measurements were later retaken with the 7A29 to verify the data taken with the 7A19.

For spectroscopic scanning experiments, the output was fed through a Keithley 417 High Speed Picoammeter, then into a Sanborn 7700 Chart Recorder. The picoammeter damped the pulsed output of the photomultiplier to provide a smoother trace to the recorder. The motor drive was connected to the spectrometer, and wavelength marks inserted onto the chart recorder by operating the marking pen on the chart recorder as the wavelength was indicated on the spectrometer dial. Uncertainty of this manual method was approximately 0.5 nanometers.

IV. Experimental Procedure

The experimental procedures used in this thesis to determine the diffusion rate and to observe some of the characteristics of the photoluminescence fall into four categories; 1) Delay Measurement, 2) Narrow Spectrum Delay Measurement, 3) Spectroscopic Scan, 4) Conversion Efficiency Measurement. Each set-up and procedure will be discussed in detail in the following sections.

Delay Measurement

A cooled sample is radiated with a laser pulse, the timing between the emitted luminescent pulse and a reference pulse is examined to determine the delay. The experimental schematic is illustrated in Figure 9.

The dewar is first filled with liquid nitrogen, then allowed to stabilize for 30 minutes. Liquid helium is then transferred into the innermost jacket of the dewar. The sample rod is inserted while the helium is being transferred. After the helium reaches an adequate fill level, the dewar is capped with a rubber stopper and a vacuum pump connected to pump down the helium beyond the laminar flow point. The temperature within the dewar surrounding the sample is 2°K at this point. The laminar flow point is easily discerned by the absence of bubbling within the liquid helium.

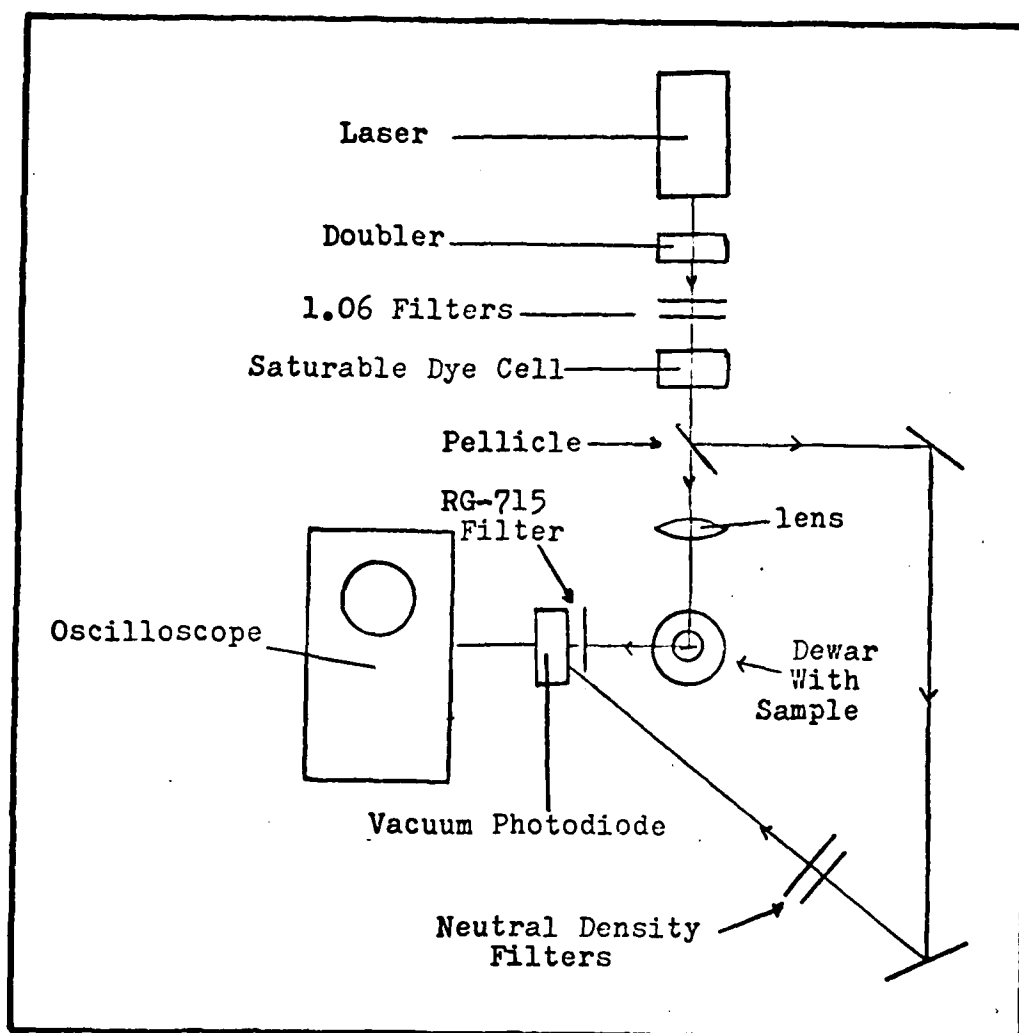


Figure 9. Delay Measurement Schematic

The dewar is then placed in the optical path as shown in Figure 9. The laser pulse is directed onto the sample by use of a short focal length lens inserted after the doubler and the 1.06 micron filters. The beam is split before the lens with a pellicle permitting a reference beam to be transmitted through an appropriate distance corresponding to the desired delay offset. This beam was directed by means of three or four mirrors and

eventually is directed to the vacuum photodiode where it enters through a small slit in the tape around the filter, which in turn is taped to the photodiode face.

The excitation beam is visually focused onto the sample but precise focus is not made at this time. The RG-715 filter/photodiode combination is placed in close proximity (3 to 4 inches) of the exit port in the dewar. The photodiode is connected to the oscilloscope by means of a low impedance coaxial cable.

The laser is turned on to a 25 pulse/sec rate and the KDP crystal tuned for maximum second harmonic output by visual means (the 532 nanometer output is green and easily visible). The reference beam is blocked and the slit in the tape covered to observe only the photoluminescent (820 nanometer and above) pulse. The focusing lens is adjusted in all three axes to provide the maximum output visible on the oscilloscope. The reference is now allowed to pass to the detector, but is generally attenuated by use of calibrated neutral density filters and by steering of the beam itself. The resultant signal appears on the scope face as in Figure 10. The first pulse is the luminescent pulse while the second pulse is the 532 nanometer reference pulse which travels the longer path length. The optical path delay is then measured by means of allowing both pulses to proceed unfiltered onto the detector. When the excitation beam is steered off

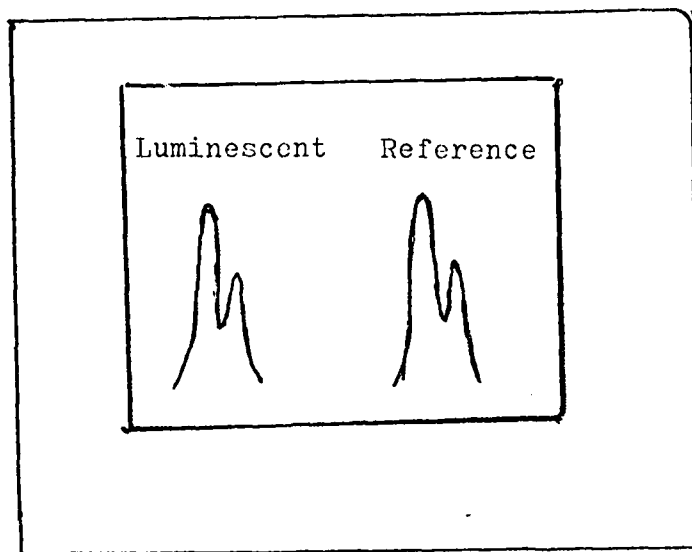


Figure 10. Typical Optical Path Delay Measurement Output

the sample, sufficient reflection occurs within the dewar windows and walls to provide the excitation reference path. For this measurement, both paths contain 532 nanometer radiation. This time delay is used as the time delay standard and its appearance is shown in Figure 11.

Both the optical path delay (both 532 nm) and the diffusion rate measurement using the luminescent and reference pulse are photographed from the oscilloscope face and compared. A delay caused by diffusion will thus appear as a contraction in the distance between pulses as illustrated in Figure 11. In order to create extremely short pulses, a saturable dye was placed before the pellicle to reduce the pulse to less than a nanosecond. The dye attenuates the intensity considerably, however the photodiode was able to detect it.

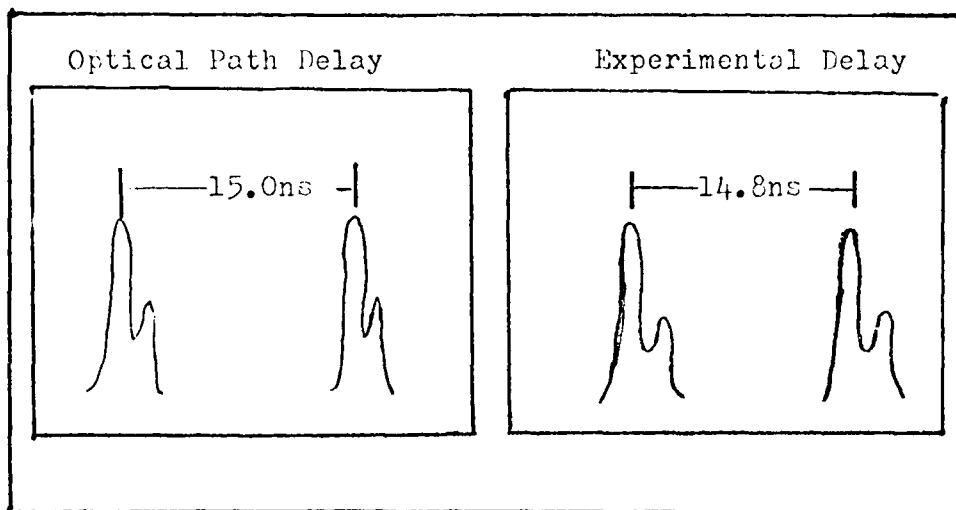


Figure 11. Illustration of Delay

Narrow Spectrum Delay Measurement

In order to fully isolate the luminescent emission from all other possible sources, a spectrometer was used in addition to the RG-715 filter. The filter allows all wavelengths longer than 750 nanometers to pass unimpeded, while the spectrometer allowed isolation to a few nanometers. The experimental set-up is very similar to that of Figure 9 and is shown in Figure 12. The primary difference is the addition of a collecting lens, spectrometer, and a photomultiplier.

The luminescent output (800 to 850 nanometers) is collected by a short focal length lens onto the entrance slit of the spectrometer. The spectrometer is coupled by means of a light-tight coupler to the photomultiplier, and a fiber-optic light path is provided to allow a reference

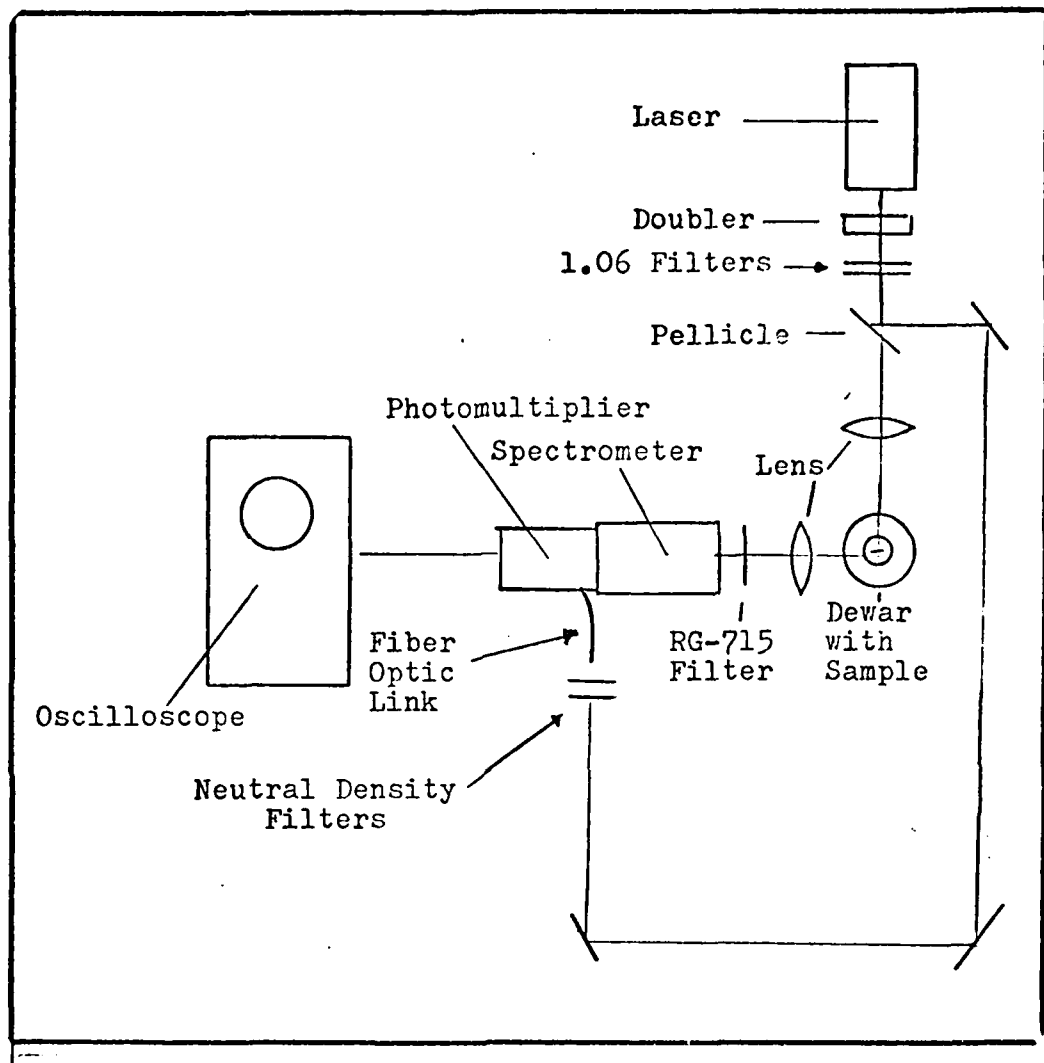


Figure 12. Narrow Spectrum Delay Measurement Schematic

signal to impinge the photomultiplier. Both entrance and exit slits were 0.5 millimeters wide.

The excitation beam is focused in the same manner as in the previous delay measurement. The exiting luminescence is focused onto the entrance slit, then the spectrometer is set to the appropriate wavelength and the luminescent pulse viewed. Both lenses are adjusted for

maximum luminescent output on the oscilloscope. The photomultiplier is two to three orders of magnitude more sensitive than the vacuum photodiode but possesses a slower response time.

The reference is allowed to illuminate the fiber optic cable after considerable attenuation by neutral density filters. The output on the scope is essentially the same as Figures 10 & 11 except the pulses are not as sharp due to the more than 1 nanosecond rise time of the photomultiplier. It is now possible to view different exciton radiation wavelengths and to ascertain that the emission observed is due to the exciton luminescence and not some other source. The optical path delay is measured by setting the spectrometer to 532 nanometers and measuring the excitation to reference delay.

Spectroscopic Scan

The previous set-up, without the reference beam path can be used as a spectrographic recording system to measure the luminescent spectrum. The system is configured as shown in Figure 13.

The dewar is brought to low temperature, then the system is aligned and tuned for maximum output as in the preceding section. A motor drive is then connected to the spectrometer and a amplifier/chart

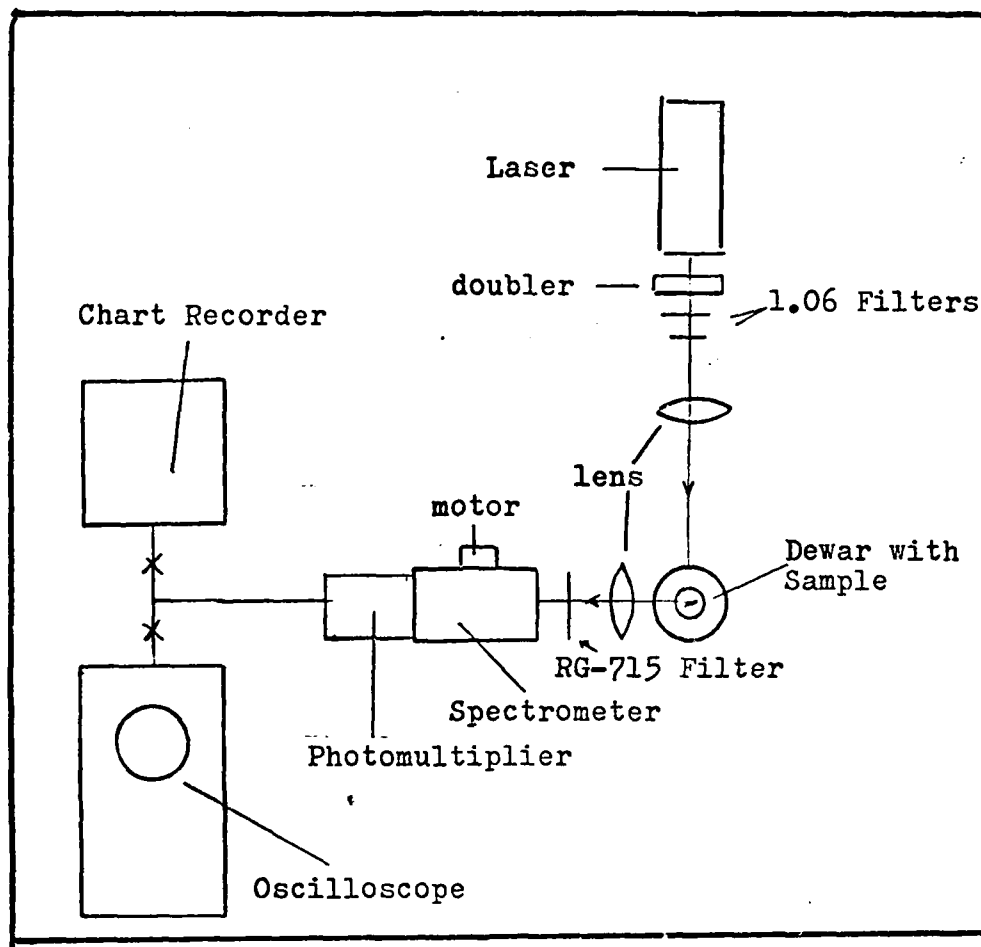


Figure 13. Spectroscopic Scan Experiment

recorder combination is connected to the photomultiplier to record the spectrum. As the motor is switched on, the spectrometer slowly scans the spectrum. The wavelength marks are placed on the chart paper by means of a second pen which is controlled by a momentary switch. This is manually activated by the experimenter as he views the spectrometer wavelength shown on the calibrated scale located on the spectrometer. This method is probably

accurate to within 0.5 nanometer. The other recorder pen records the averaged photomultiplier output.

The oscilloscope can be used to view low level signals that are virtually the same level as the photomultiplier noise. In this way, the spectrometer can be made extremely sensitive. The spectrometer is normally scanned manually when the oscilloscope is used.

Conversion Efficiency Measurement

The relative conversion efficiency of the 532 nanometer excitation beam to the 820 nanometer luminescent emission was measured by use of the system shown in Figure 14.

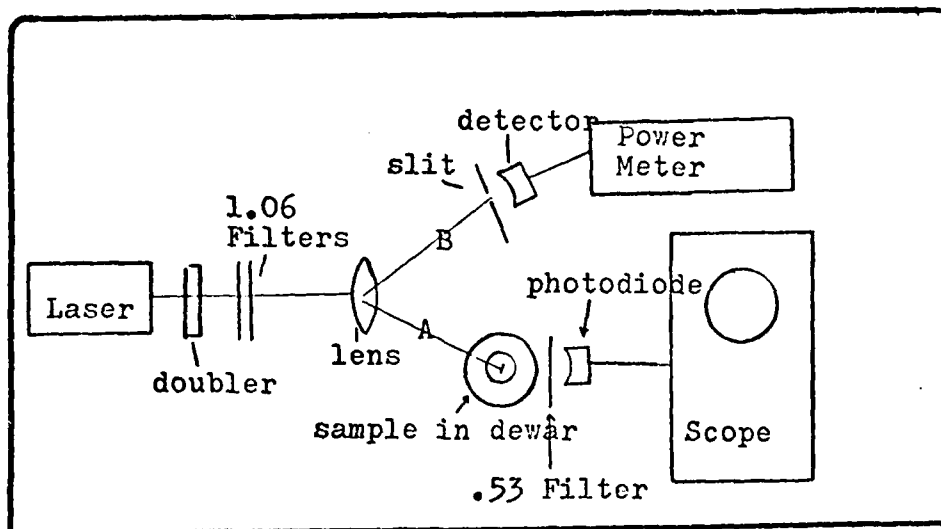


Figure 14. Conversion Efficiency Measurement Schematic

The system is essentially that of the delay measurement without the reference beam. The beam is set up to

traverse path A (Figure 14) and the lens adjusted to produce maximum luminescent intensity at the photodiode. The resulting pulse is photographed on the oscilloscope. The detector area and distance from sample are measured to determine the solid angle subtended.

Then the system is reconfigured to traverse path B (Figure 14). A slit is adjusted to the same size as the sample and the average power measured using a Scientech power meter. In this manner, both the incident energy and luminescent energy can be compared to yield an order of magnitude estimate of efficiency.

V. Experimental Results/Discussion

The primary objective of this thesis was to investigate the possibility of determining the diffusion rate of holes in n-GaAs. The experimental procedures detailed in Chapter IV were developed and utilized to produce data in these areas; 1) Diffusion rate determination by delay measurements, 2) Spectroscopic scans to study luminescent spectra and possible delay differences between different allowed exciton levels, 3) Conversion efficiency of 532 nanometer excitation to 820 nanometer luminiscence.

Diffusion Rate Determination

Large quantities of data were taken using the delay and narrow spectrum delay measurement procedures detailed in Chapter IV. A sampling is contained in Appendix A. Numerous oscilloscope time scales and different optical path delays were used in order to acquire the best data. A representative example used to illustrate the experimental results is shown in Figure 15. A number of observations can be made:

- 1) The experimental delay is hardly visible, certainly in the range of 350 picoseconds or less. It shows up as less than a millimeter wide in the scope photographs.

- 2) The luminescence pulse (left pulse on photo B

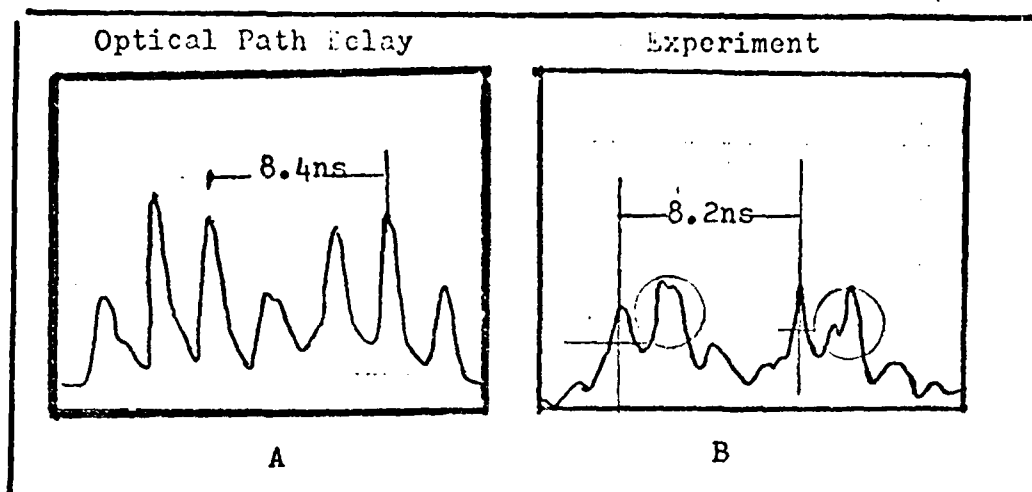


Figure 15. Typical Experimental Result

on Figure 15 within circle area) is not capable of following abrupt slope changes. This is apparent in a large number of scope photographs. The laser pulse is the right pulse on photo B, Figure 15.

3) Some photographs show an apparent broadening within the luminescence pulse compared to the excitation pulse. (The crosses on photograph B, Figure 15) It is on the order of 500 picoseconds and only visible with the fastest scope amplifier and shortest time scale.

These observations led the researcher to view this experimental technique as valid only to set an upper bound on the delay time and usable only to generate an estimate of the diffusion rate. The measurement equipment is being pushed temporally to the limit of

response. The excitation pulse and the vacuum photodiode are both limited to 250 picosecond response at best.

Determination of diffusion rate by observation 1 is only an order of magnitude approximation. As shown in the computer plots in Appendix B, the rise time is in the 100 to 400 picosecond range. Such differences are impossible to judge in the scope photographs.

Observation 2, although interesting, is not very useful, inability to follow slope changes is not readily translatable into delay times. The cause of this effect appears to be the additive interference of the delayed trailing edge of the first pulse with the leading edge of the next pulse.

Observation 3 yields the best possibility of determining diffusion rates. The broadening effect of pulses by diffusion is in the 500 picosecond range and is somewhat easier to measure on the scope photographs. This broadening can be compared to the various computer generated plots, specifically those generated using Equation (32). The input excitation was modeled by a rectangular pulse of 500 picoseconds width. The halfwidth of the luminescent output is then compared to the halfwidth of the computer plots in Appendix B (Plots B-9 to B-13) and a value of D can be estimated. This concept is illustrated in Figure 16.

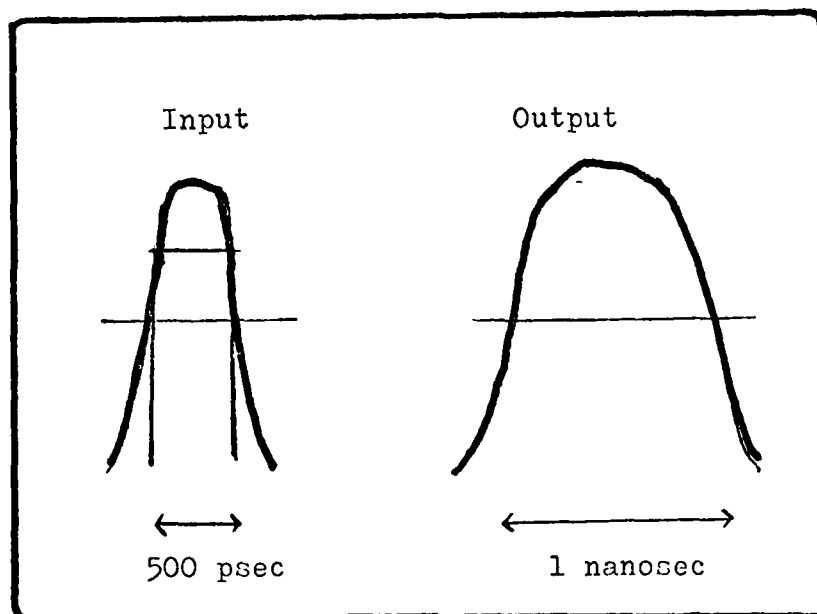


Figure 16. Typical Broadening

Comparison with broadening on the theoretical computer plots yielded the best match when $D=100 \text{ cm}^2/\text{sec}$. It should be noted that the only broadening source in this analysis is assumed to be diffusion.

Spectroscopic Study

Spectroscopic studies were performed using the procedures outlined in Chapter IV. A typical spectrum is shown in Figure 17. The spectrum contains the various exciton combinations from 818 nanometers to 832 nanometers. The spectrum appears smooth because the spectrometer cannot resolve beyond 1 or 2 nanometers. Note that the

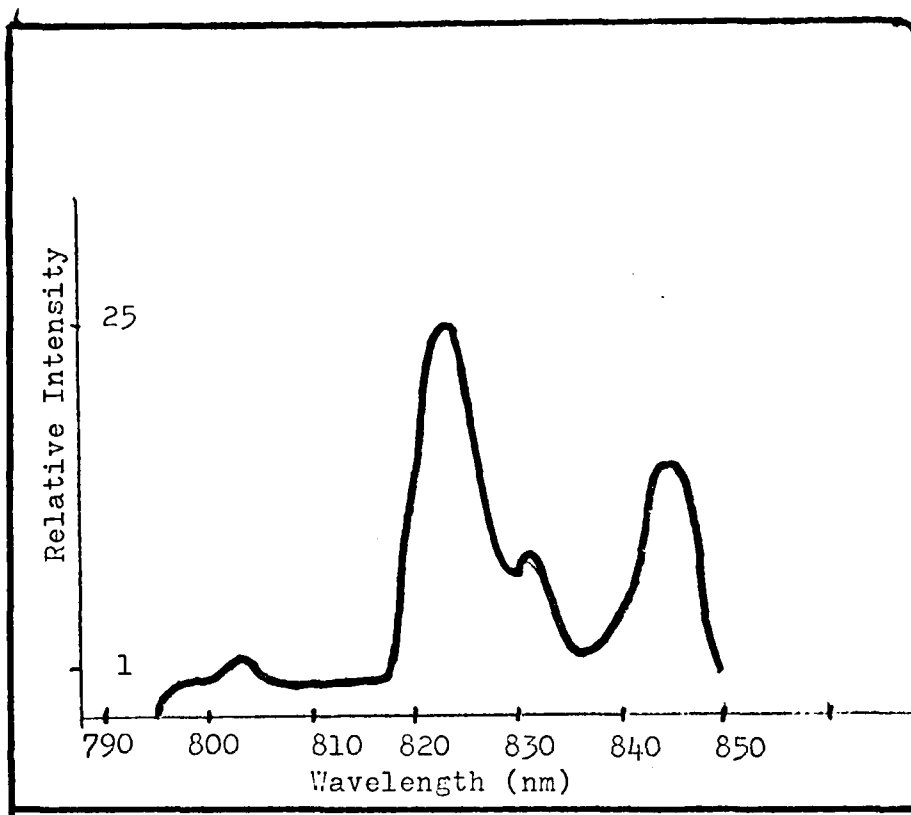


Figure 17. Spectroscopic Spectrum (Scaled by photomultiplier response)

presence of a phonon replica at 843 nanometers (36.4 meV away in energy from 823 nanometers) is quite evident. By far the most interesting result was the unexpected presence of higher-than-band-gap-energy transitions. The band gap corresponds to 815.7 nanometers in this material. By setting both the oscilloscope gain and the photomultiplier voltage to maximum, it was possible to view spectral lines down to 795 nanometers. The amplitude of these

transitions was 25 times lower than the expected exciton transitions above 818 nanometers.

To the best of the author's knowledge higher-than-band-gap-energy transitions have not been observed before. This experiment utilized high incident laser power and extremely sensitive detection methods. Short lived transitions in the 250 picosecond range could therefore be observed. Possible theoretical explanation for this phenomenon can be illustrated in Figure 18 below.

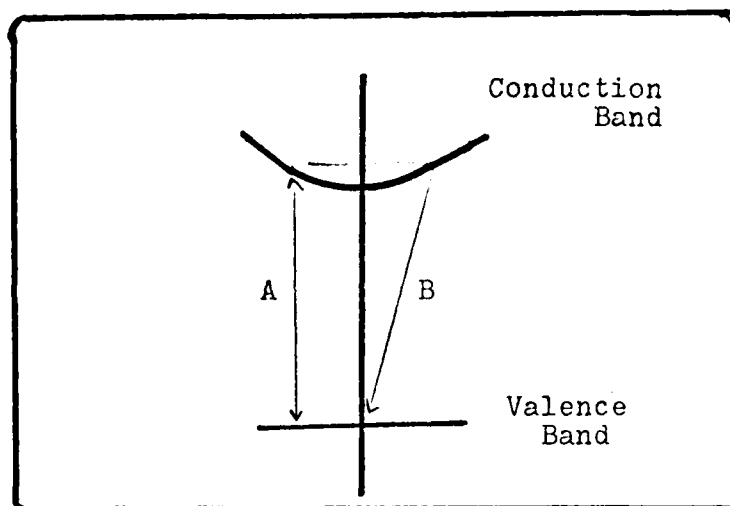


Figure 18. Higher-than-Band-Gap Radiation

The Fermi level in the degenerate region is in the conduction band. The incident photon bombardment may create a momentary "super-degenerate" zone in the absorption region. The subsequent downward transitions can take two forms. One (Labeled A in Figure 18) is a direct transition from the top of the Fermi level to an equal momentum point in the valence band. The other (Labeled B)

transition is a phonon assisted transition from the Fermi level to the zero momentum point in the valence band.

Either of these two transitions are not very probable. However the type A transition is slightly more likely than the B transition. Experimental results do tend to verify these assumptions, the observed transitions were at least 25 times weaker than the exciton emissions and there was an apparent peak in the data at 804 nanometers which may have been the Fermi level to valence band direct transition (labeled A).

Spectroscopic studies using photographic plates and continuous wave sources probably cannot see this radiation because the crystal reaches thermal equilibrium (zero momentum) in an extremely short time. Continuous sources also contain 3 to 4 orders of magnitude less optical power than the pulsed laser source used in this experiment.

Scattering in the spectrometer from the 818-823 nanometer radiation was considered as a possible source but quickly discounted. A scattering measurement (described in Appendix D) was performed resulting in scatter of 0.05% at 10 nanometers away from an intense spectral line. It was therefore assumed the unexpected

radiation came from within the sample.

Delay measurements were performed at different exciton wavelengths resulting in absolutely no observable difference in delay. This would be the case assuming all excitons are annihilated at the active-buffer interface.

Conversion Efficiency

The relative conversion efficiency of 532 nanometer excitation to 820 nanometer luminescence was examined using the experimental procedure given in Chapter IV. The average laser power was measured to be 5 milliwatts. Dividing by the repetition rate of 25 pulses/sec yielded an energy per pulse of 2×10^{-4} joules.

The voltage pulse observed on the oscilloscope was approximated to be an average of 50 millivolts high in a 10 nanosecond pulse width (treated as rectangular). Dividing by the 50 ohm scope impedance gives a 1 milampere current. The sensitivity curve for the F4000 photodiode requires 1 watt input for 1 milampere output. The area of the photodiode cathode was 4 square inches and the detector was 3 inches away from the sample resulting in a solid angle of 0.43 steradians. Assuming the luminescence is emitted in 4 π steradians means the luminescent output is 29 watts. Multiplying by the time

period of the pulse yields a luminescent energy of 2.9×10^{-7} joules per laser pulse.

The efficiency is defined by this equation

$$\text{Efficiency} = \frac{\text{Energy (820nm)}}{\text{Energy (532nm)}} \times 100 \quad (33)$$

and
results in an efficiency of 0.144%

VI. Conclusions

On the basis of the experimental results and theoretical analysis carried out for this thesis project, the following conclusions have been reached.

1. For the sample thickness in this experiment, the procedure utilized can only give an approximate estimate of the diffusion rate in n-GaAs. The experimental apparatus is being pushed to the limit of its' response. An estimate of $D=100\text{cm}^2/\text{sec}$ is given. Reasonable diffusion coefficients in the room temperature range are $50-67\text{ cm}^2/\text{sec}$ (Ref 3:638). A slight increase of this coefficient can be expected at lower temperatures. An upper bound of 350 picoseconds absolute delay is evident.
2. Spectral luminescent output is as expected with all exciton wavelength emissions appearing to yield the same delay from excitation signal to exciton decay.
3. Unexpected, low intensity radiation at higher than band gap energy was observed and possible explanations tendered.
4. Relative conversion efficiency from the 532 nanometer excitation to the luminescent 820

nanometer exciton decay emission is 0.144%, but visible due to the high input power applied by the Q-switched laser excitation.

VII. Recommendations

Based on theoretical calculations and observations during the conduct of the experiment, the following recommendations are offered for possible study:

1) Thicker samples could be constructed given adequate preparation time. Theoretical plots shown in Appendix B predict delay times of 2 nanoseconds for sample thicknesses of 8 microns or more. Delays of this scale would be readily apparent on the experimental system used in this thesis. The only drawback to this approach is that the intensity of the luminescent output would necessarily be less and may not be readily detectable. Rough calculations show it to be a factor of 75 times lower for an 8 micron sample.

2) Should the approach outlined above be invalid due to intensity considerations and it becomes necessary to investigate samples of only 4 microns or less (typical active layers in semiconductor devices are less than 4 microns), an alternative is presented.

Use of a good mode-locked laser could provide excitation pulses of 50 picoseconds duration or less. The detection system used in this thesis would be inadequate for this time scale. Use of a two photon detector is recommended. The basic experimental system is diagrammed in Figure 19. (Proposed system)

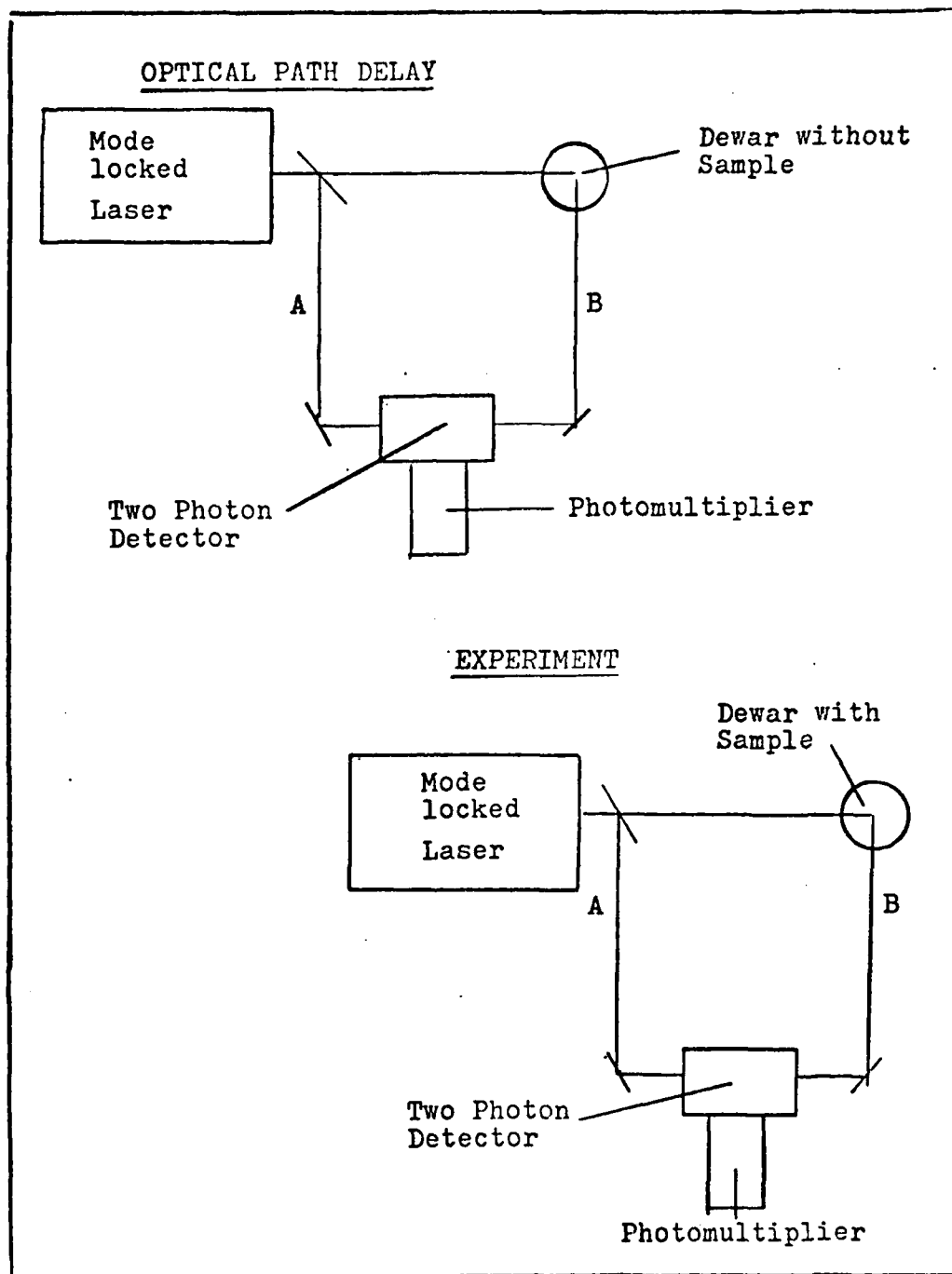


Figure 19. Mode-locked Laser/2 Photon Detection System

The two photon detector is composed of a molecule selected to respond to the additive energy of two photons.

(Ref 6:317)

For example, for the reference optical path delay, the molecule would respond by luminescence to two 2.33 eV (two 532 nanometer) photons. A diagrammatic representation of a two photon process is shown in Figure 20.

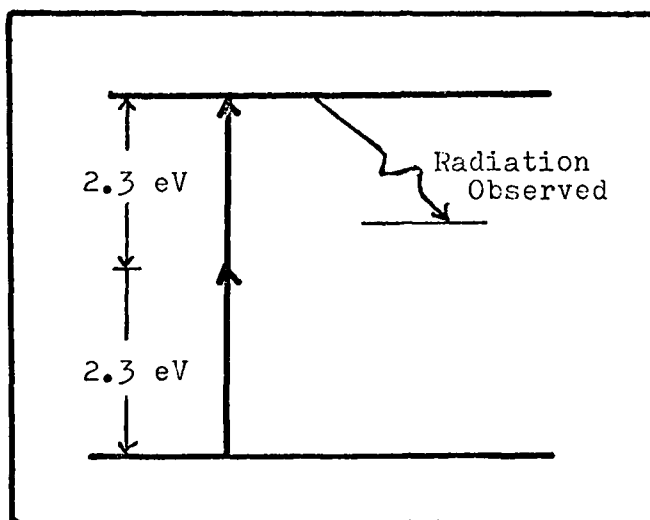


Figure 20. Two Photon Process

The photons must arrive at the same time (within the pulse width) to produce an output visible by a photomultiplier. The respective optical paths (A&B in Figure 19) can be made equal by moving a mirror or the detector until a signal is detected. The sample is then placed into the dewar and irradiated. The detector or mirror is moved until the luminescent pulse caused by a 3.84 eV process (532&820 nanometer) is detected. The distance moved can be directly converted into a time delay. (1 meter=3 nanoseconds)

It will probably be impossible to find a molecule

that will respond to both a 4.66 eV and a 3.84 eV two photon process, therefore two materials will have to be selected.

Use of this method could result in delay determination to within 50 picoseconds.

Bibliography

1. McKelvy, John P. Solid State and Semiconductor Physics (Out of Print). New York: Harper & Row (1966)
2. Reynolds, D. et al. "Sharp Line Emission Spectra From GaAs FET-like Structures", Journal Electronic Materials, Vol 7:263 (1978)
3. Casey, H.C. and Frank Stern. "Concentration-Dependent Absorption and Spontaneous Emission of Heavily Doped GaAs", Journal of Applied Physics, Vol 47, No 2:631-643 (February 1976)
4. Ettenberg, M. "The Effect of Reabsorbed Radiation on the Minority-Carrier Diffusion Length in GaAs", Applied Physics Letters, Vol 30, No 4: 207-210 (February 1977)
5. Kittel, Charles. Introduction to Solid State Physics (Second Edition). New York: John Wiley & Son Inc (1960)
6. Crank, J. The Mathematics of Diffusion (Second Edition) London: Oxford University Press (1976)
7. Bloembergen, N. and M.D. Levenson. "Doppler-Free Two Photon Absorption Spectroscopy", High-Resolution Laser Spectroscopy, (Edited by K. Shimoda). New York: Springer-Verlag (1976)

Appendix A

Experimental Data

A series of oscilloscope photographs is reproduced to permit the reader to better understand the capabilities and limits of the measurement system. It should be noted that laser pulses vary in amplitude somewhat from pulse to pulse.

Most figures are presented in pairs with the optical path delay on the left and the experimental delay on the right. Particular experimental parameters such as time scale, filter method, and type of detector will be indicated.

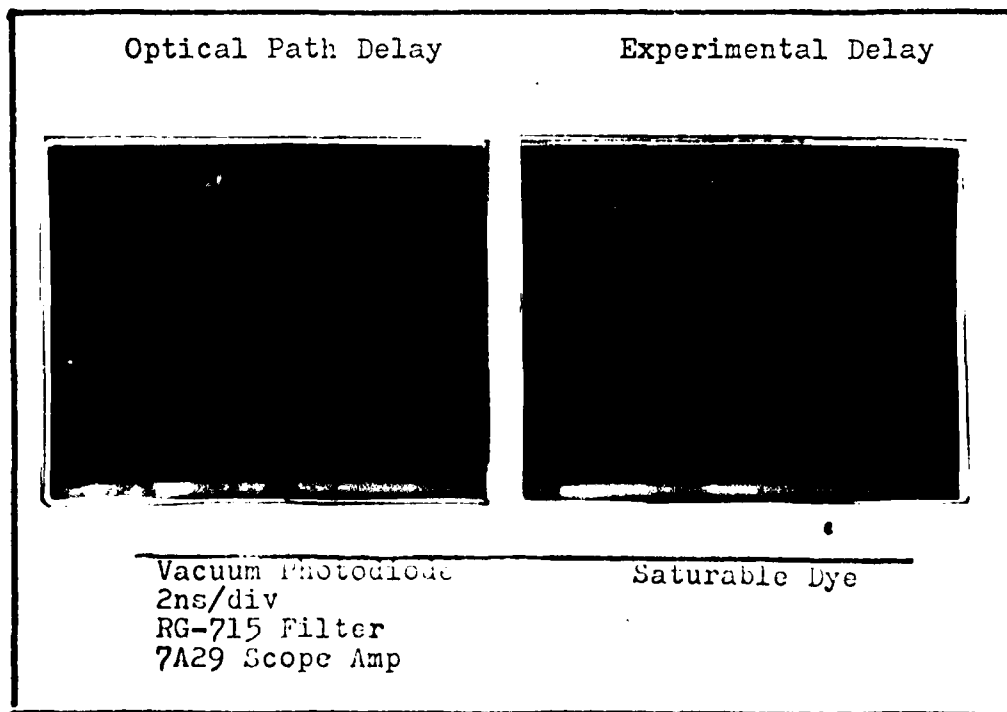


Figure A-1. Experiment Photograph

Things to note:

- Figure A-1 This is the original for Figure 15.
Both a slight delay and broadening are visible. Pulses are less than a nanosecond wide. Inability to follow slope evident.
- Figure A-2 Both are taken using the ITT photomultiplier
A-3 and use the full 10 nanosecond laser pulse.
Minimal broadening visible and no observable delay.
- Figure A-4 This figure represents the relationship of the above band gap emission to the exciton emission. The noise pulse is 30 millivolts high. The above band gap pulse gradually becomes higher than the noise pulse at 795 nanometers and averages less than 200 millivolts up to 818 nanometer. There is an apparent peak at 804 nanometers as shown in the figure. (unfortunately no photographs of 800 nanometers taken, just the level was observed in this region). The height of the exciton radiation at 823 nanometers was 2 volts for a 10 to 1 ratio to the above-band-gap radiation. The spectrometer is 2.5 times more sensitive at 800 than 823 nm (see Appendix C) resulting in an overall intensity of 25 more intense.
- Figure A-5 Representative of data using fast detector,
A-6 saturable dye, and 600 MHz scope amp. Some delay, broadening, and inability to follow slope visible.
- Figure A-7 Photographs using longer time scale show
A-8 total laser pulse reproduced. No delay observable.

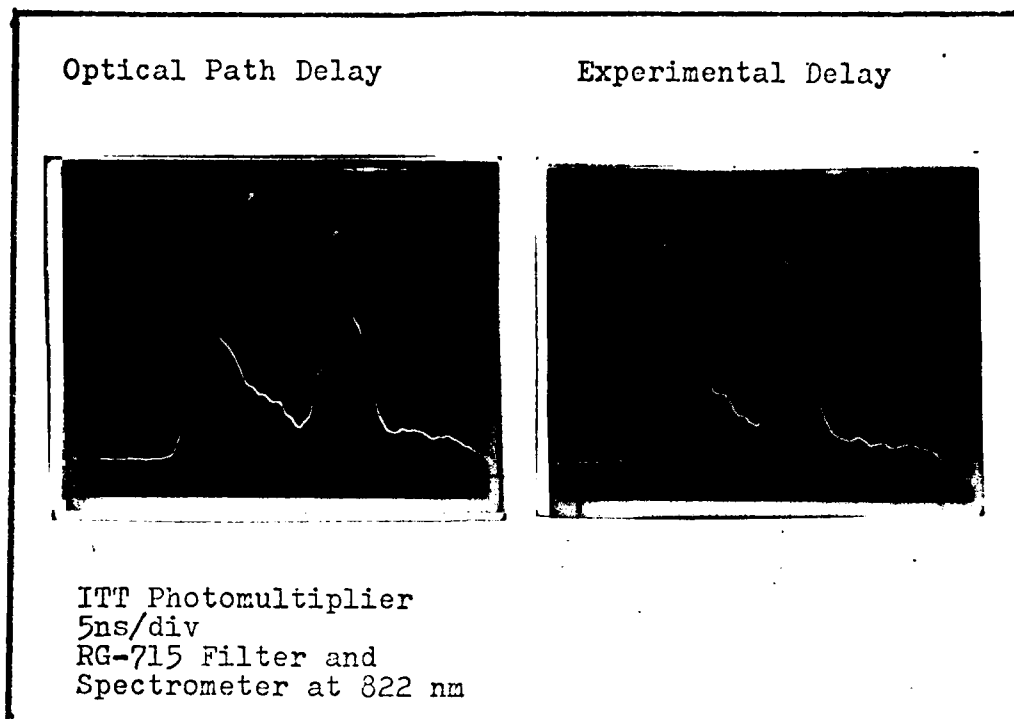


Figure A-2. Experiment Photograph

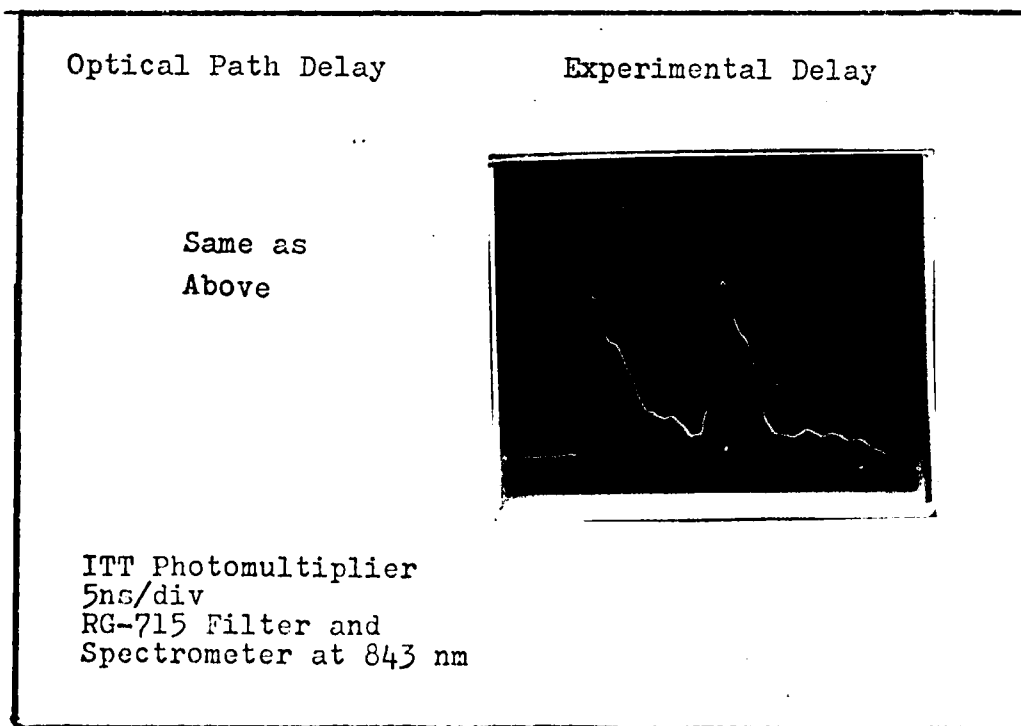


Figure A-3. Experiment Photograph

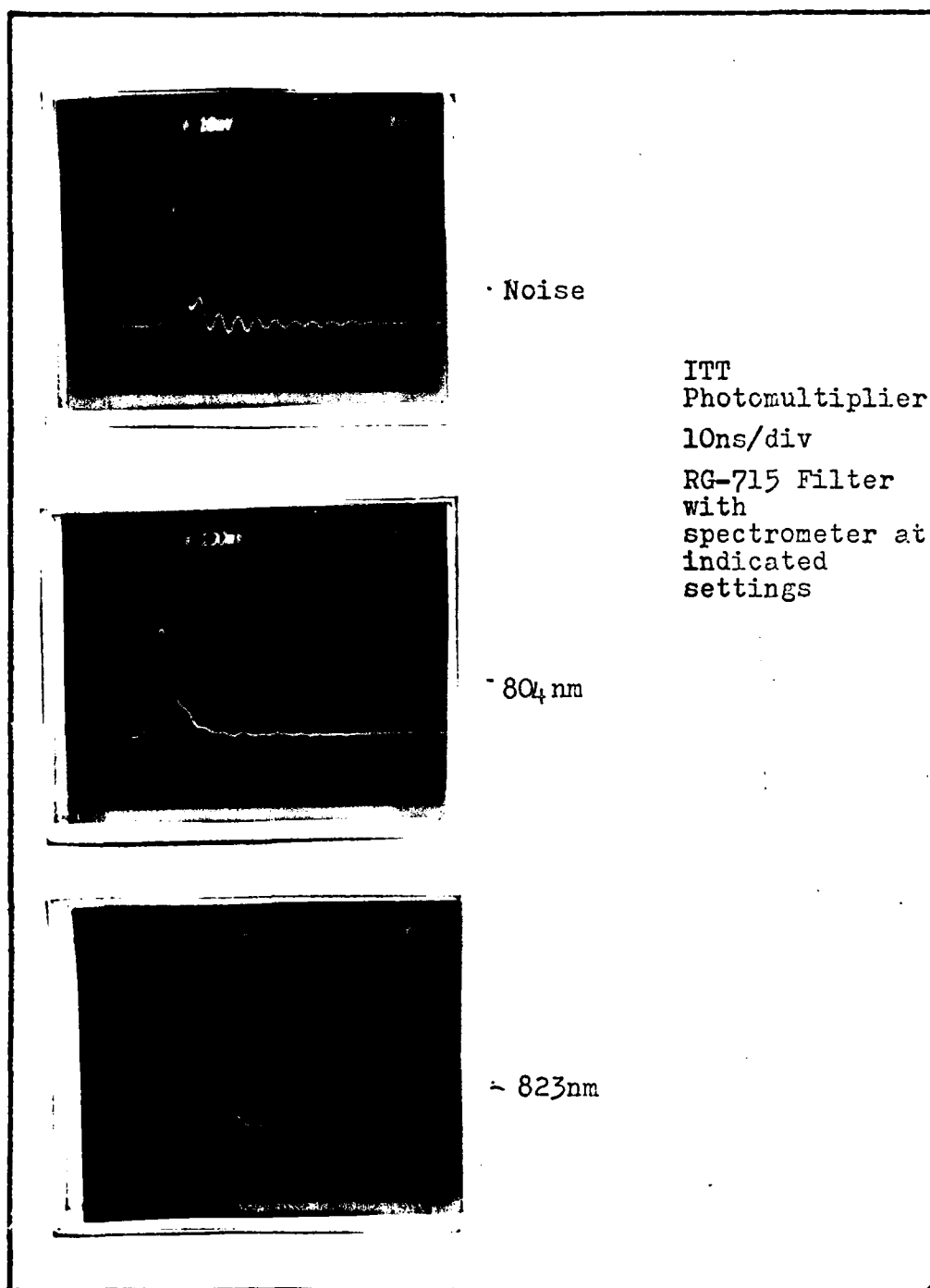


Figure A-4. Experiment Photograph

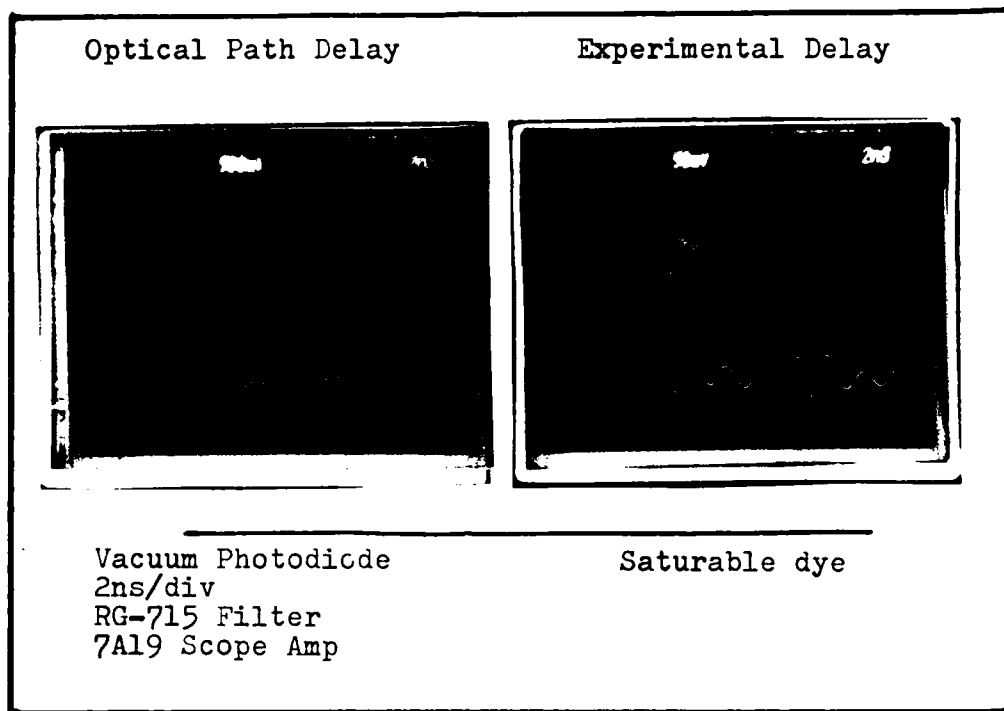


Figure A-5. Experiment Photograph

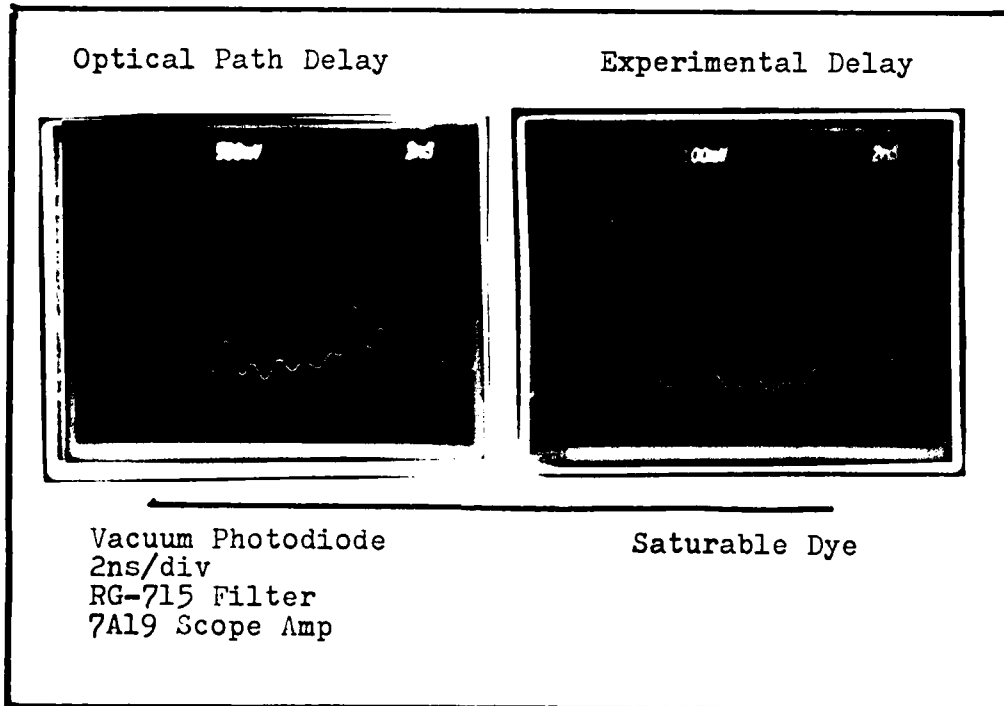


Figure A-6. Experiment Photograph

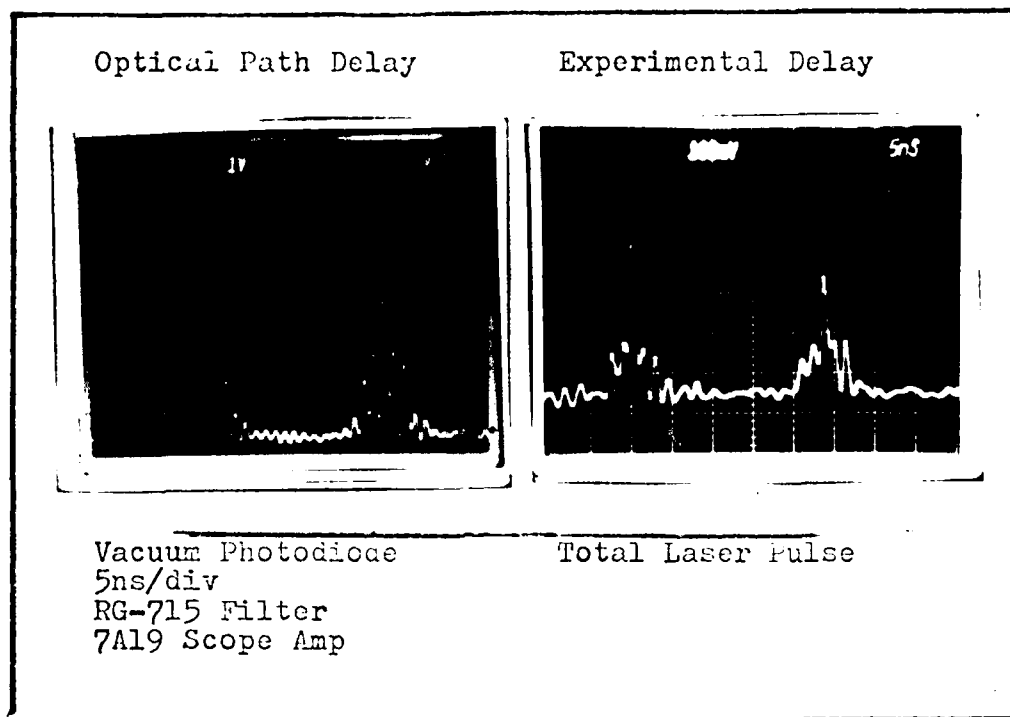


Figure A-7. Experiment Photograph

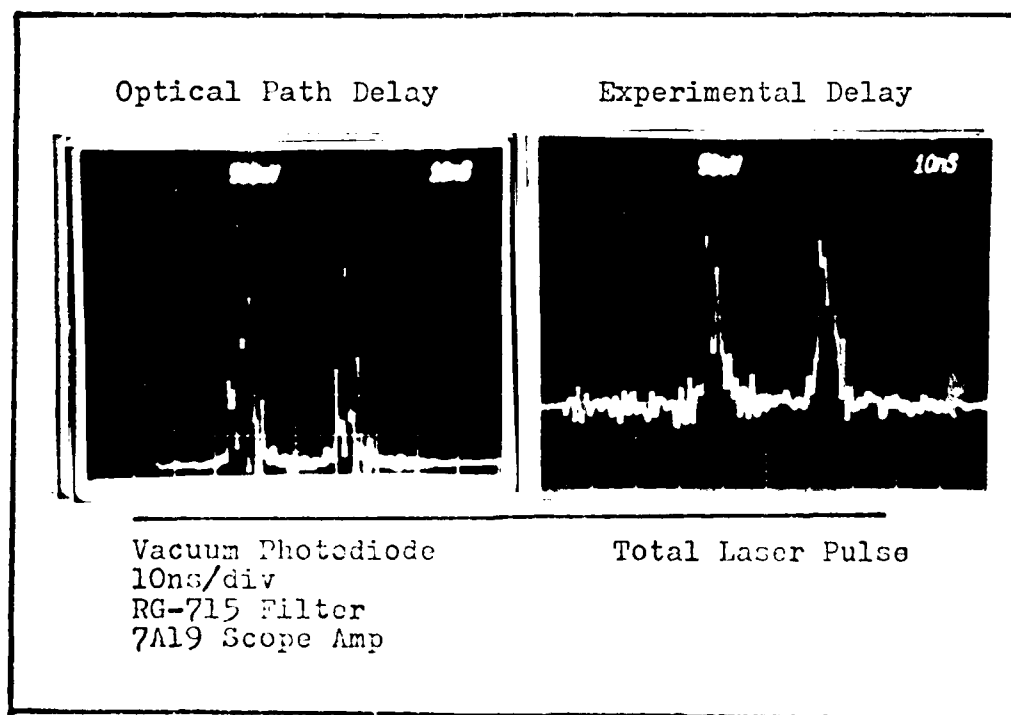


Figure A-8. Experiment Photograph

Appendix B

Computer Plots of Solution to the Diffusion Equation

Computer plots of the diffusion equation solution in Chapter II were made using Eq (28) reproduced here.

$$I_{out} = \alpha \beta I_0 \frac{L}{\sqrt{\pi D t}} e^{-L^2/4Dt} \quad (28)$$

The plots were generated using the program listed in Figure B-1. Various plots were made using different values of diffusion rate (D) and sample depth (L).

A check on the plots was made by calculating the location of the maximum point. This can be derived by time differentiation of Eq (28) and setting it equal to zero.

Differentiation of Equation (28) after cancellation of all extraneous terms yields

$$L^2/4t^{7/2} D + 3/2t^{5/2} = 0 \quad (30)$$

then solving for t produces

$$t_{max} = L^2/6D \quad (31)$$

where L=sample thickness
D=diffusion rate

The plots are presented in the order indicated in Table I. This table also contains values of rise time, time to maximum, and halfwidth all read from each plot.

Computer plots of the diffusion equation solution using a rectangular input function (Eq(32)) were also made. Equation (32) is reproduced below:

$$I_{OUT} = \left[\operatorname{ERFC}\left(\frac{k}{2\sqrt{Dt}}\right) - \operatorname{ERFC}\left(\frac{k}{2\sqrt{D(t-t_1)}}\right) u(t-t_1) \right] \quad (32)$$

The plots were generated using a program shown in Figure B-9. Various plots for different values of diffusion rate constant (D) and sample depth (L) were made. Table I contains values of rise time, time to maximum, and halfwidth all read from each plot (B-10 to B-14).

Table I
Computer Data on Diffusion Equation Solution

Figure #	Diffusion rate D (cm^2/sec)	Thickness L (microns)	Rise Time (nanosec)	Time to Max (nanosec)	Halfwidth (nanosec)
B-2	25	4	0.9	1.0	2.5
B-3	50	4	.4	.5	1.3
B-4	100	4	.3	.35	.55
B-5	200	4	.15	.17	.35
B-6	50	8	1.7	2.0	5.0
B-7	100	8	.9	1.0	2.5
B-8	50	10	3.0	3.5	6.0
B-10	50	4	.8	.9	1.6
B-11	100	4	.4	.7	1.0
B-12	200	4	.4	.6	.7
B-13	50	8	1.5	2.5	5.0
B-14	100	8	1.0	1.3	2.0

```

100. PROGRAM GAB (INPUT,OUTPUT,PLOT)
110. DIMENSION F(30),G(30)
120. PRINT*, 'ENTER TIME SCALE, DIFFUSION RATE'
130. PRINT*, 'ENTER LENGTH'
140. READ*, A, D, R
150. PRINT*, 'TIME SCALE', A, 'DIFFUSION RATE ', D, 'LENGTH ', R
160. C=A/20
170. PI=3.1415926
180. DO 10 I=1,20
190. E=I
200. E=I
210. F(I)=C/E
220. G(I)=R/(2*SQRT(PI*D*(F(I)**3)))*EXP(-(R**2)/(4*D*F(I)))
230. PRINT*, 'THE VALUE OF G(I) IS ', G(I)
240. 10 CONTINUE
250. CALL PLOT(0.,0.,-3)
260. CALL SCALE(F,0.,20,1)
270. CALL SCALE(G,7.,20,1)
280. CALL AXIS(0.,0.,4*TIME,-4,6.,0.,F(21),F(22))
290. CALL AXIS(0.,0.,15*RELATIVE OUTPUT,15,7.,90.,G(21),G(22))
300. CALL LINE(F,0.,20,1,1,4)
310. CALL SYMBS(3.5,6.,-14,12*DIFFUSION EQ,0.,14)
320. CALL PLOTEN
330. END
..

```

Also used are ASD Library Routines

TEKLIB & PREVIEW

Figure B-1. Computer Program

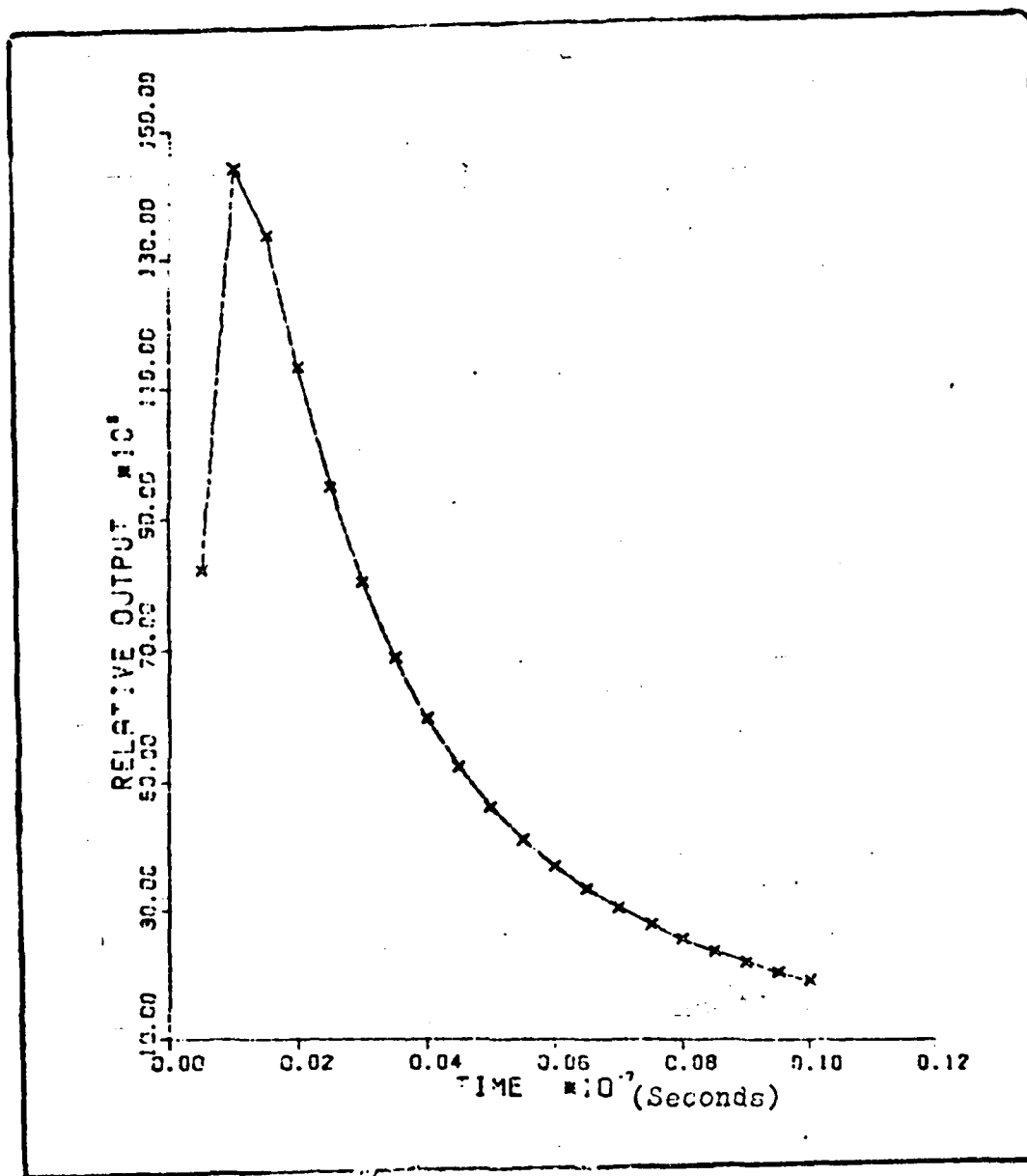


Figure B-2. Computer Plot (D=25, L=4um)

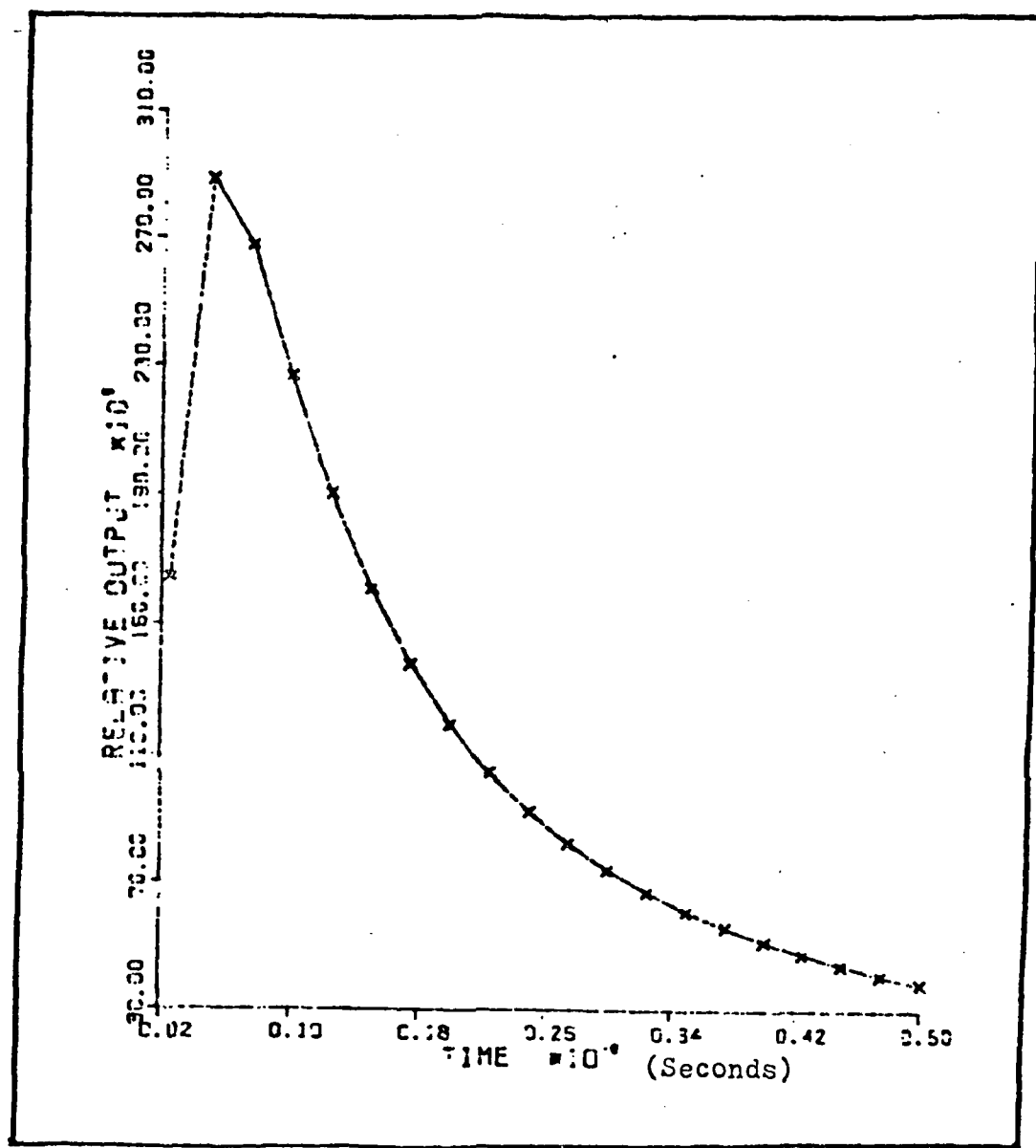


Figure B-3. Computer Plot (D=50, L=4um)

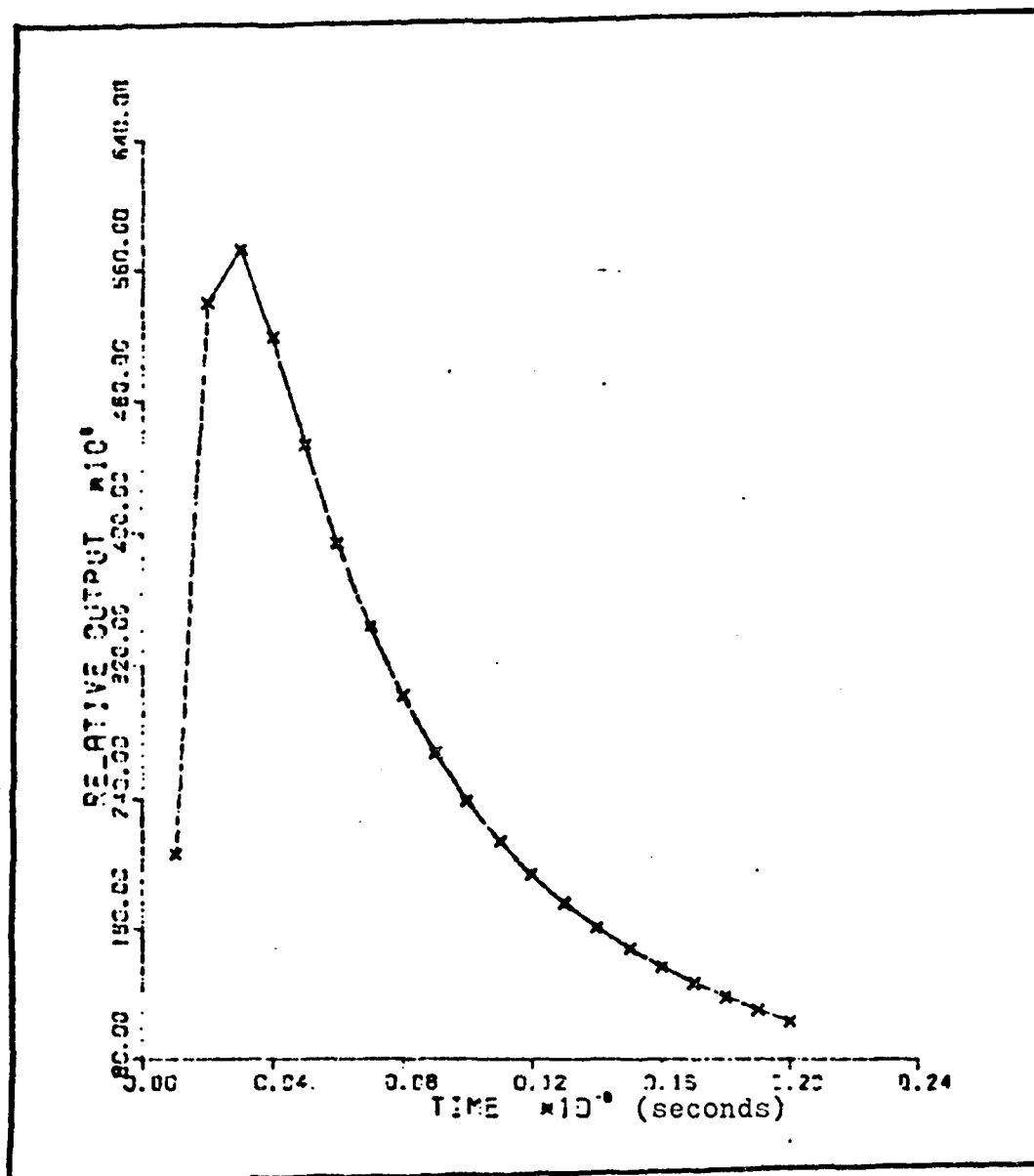


Figure B-4. Computer Plot ($D=100, L=4\mu m$)

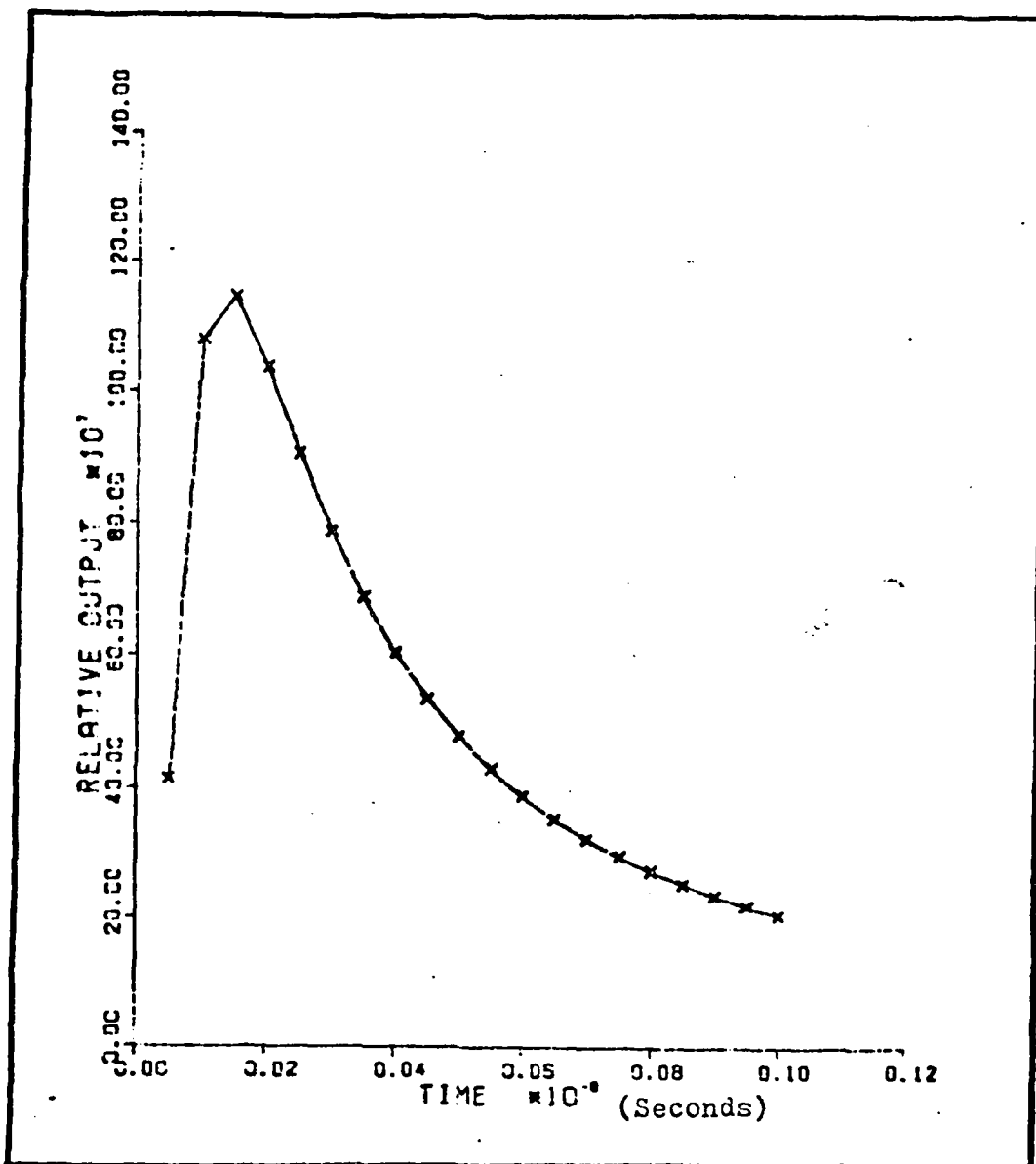


Figure B-5. Computer Plot ($D=200$, $L=4\mu m$)

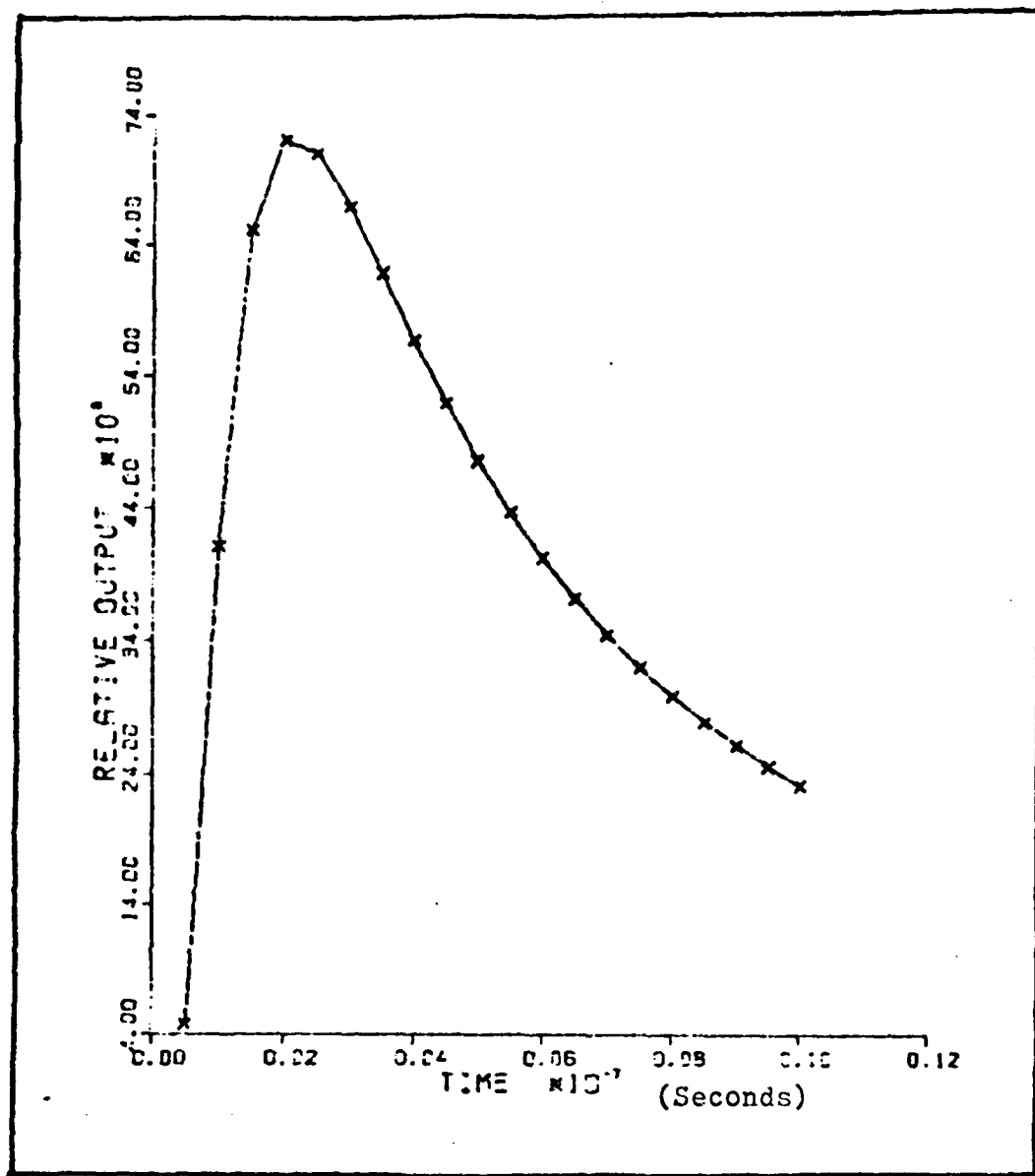


Figure B-6. Computer Plot ($D=50$, $L=8\mu m$)

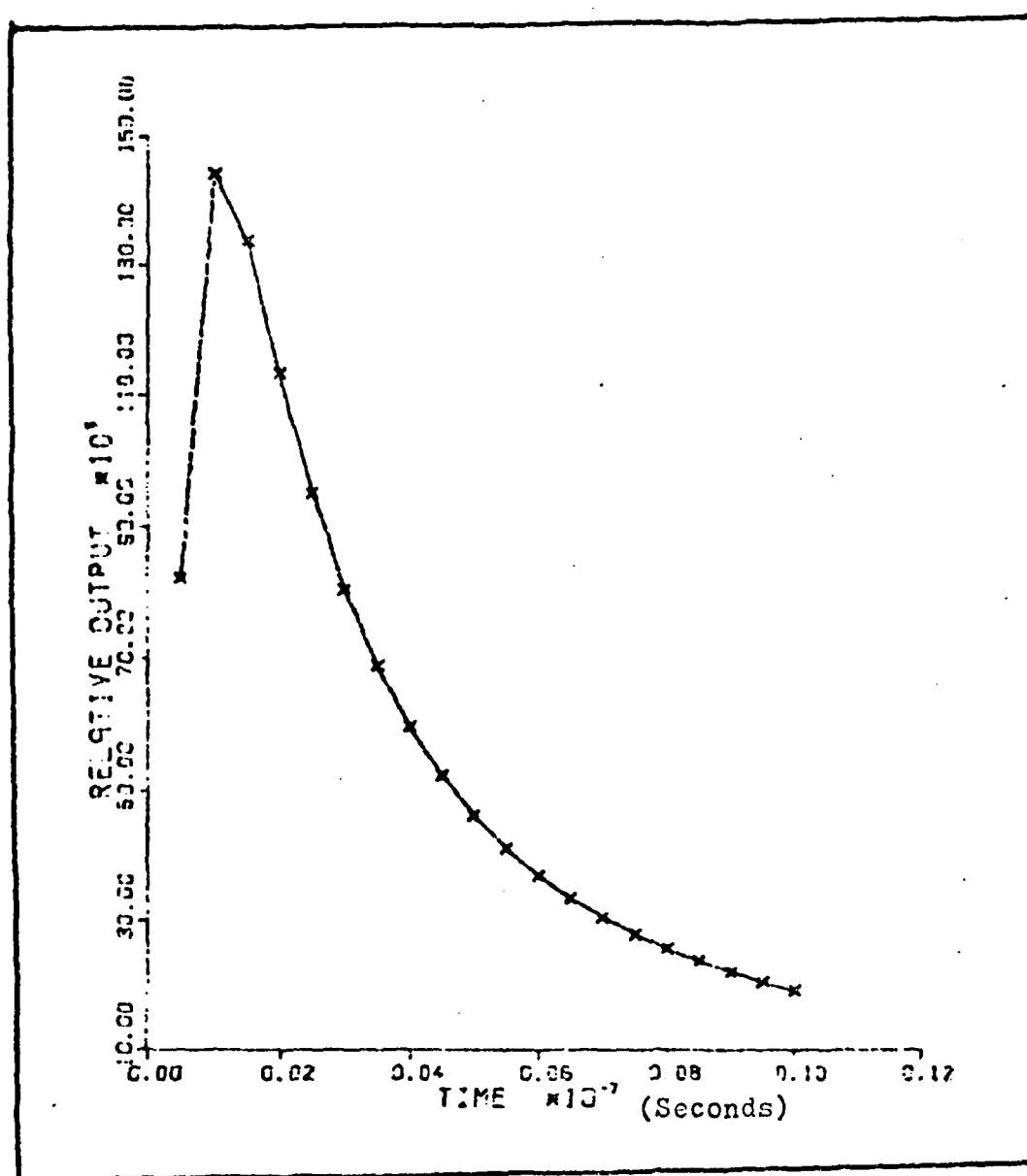


Figure B-7. Computer Plot (D=100, L=8um)

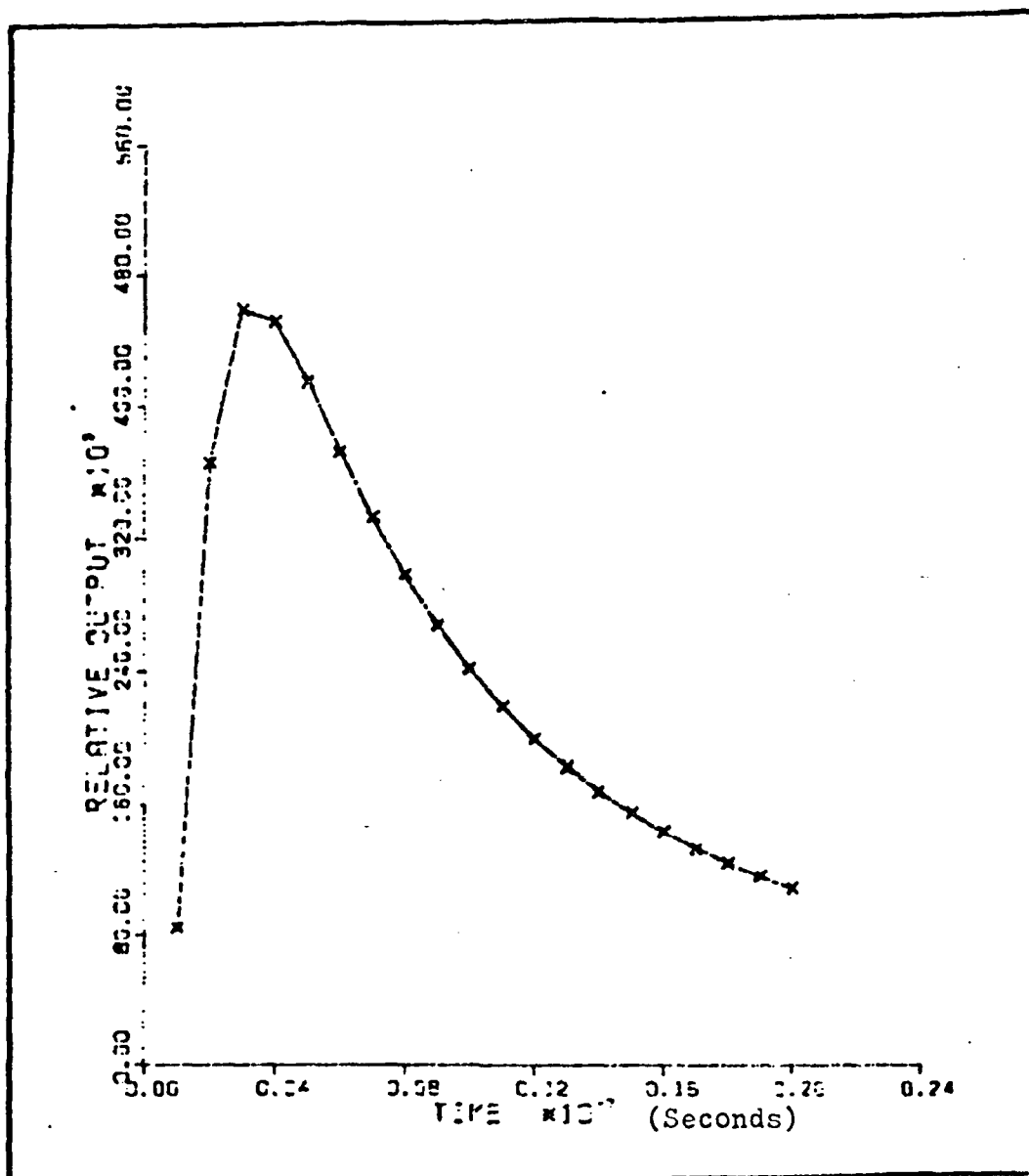


Figure B-8. Computer Plot ($D=50$, $L=10\mu m$)

```

100. PROGRAM GAS(INPUT,OUTPUT,PLOT)
110. DIMENSION F(45),G(45),GB(45),GA(45)
120. PRINT*, "ENTER TIME SCALE"
130. READ*, A
140. R=4E-4
150. PI=3.1415926
160. C=A/40
170. DO 50 I=1,40
180. E=I
190. F(I)=C+E
200. GA(I)=ERFC(R/(2*SQRT(50*F(I))))
210. IF(F(I)-(5E-10))10,10,20
220. 10 GB(I)=0
230. GO TO 40
240. 20 GB(I)=ERFC(R/(2*SQRT(50*(F(I)-(5E-10)))))
250. 40 G(I)=GA(I)-GB(I)
260. 50 CONTINUE
330. CALL SCALE(F,6.,40,1)
340. CALL SCALE(G,7.,40,1)
350. CALL AXIS(0.,0.,4*TIME,-4,6.,0.,F(41),F(42))
360. CALL AXIS(0.,0.,15*RELATIVE OUTPUT,15,7.,90.,G(41),G(42))
410. CALL LINE(F,G,40,1,1,4)
450. CALL PLOT(N)
490. END
..

```

Also used are ASD Library Routines
TEKLIB & PREVIEW

Figure B-9. Computer Program

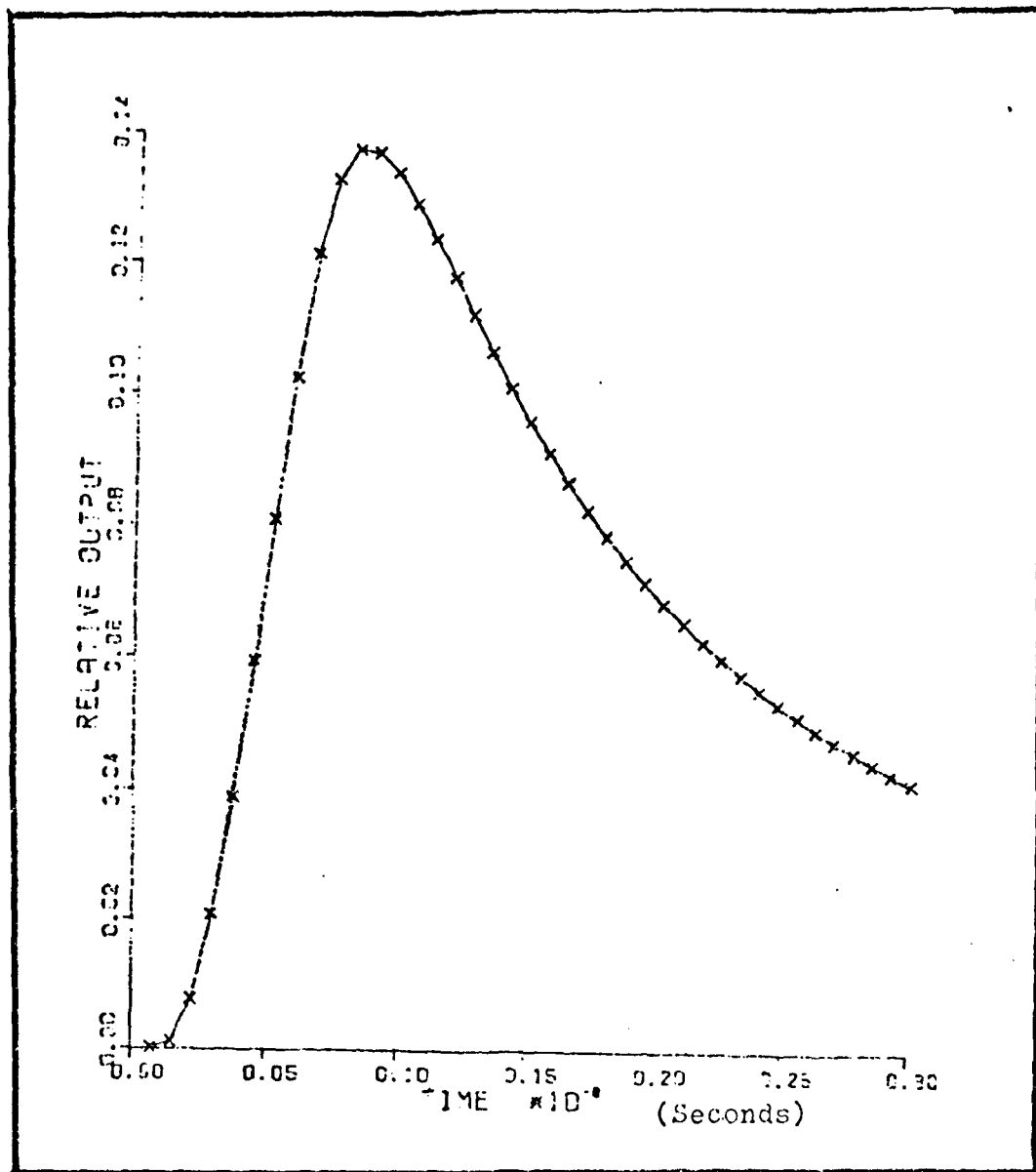


Figure B-10. Computer Plot ($D=50$, $L=4\mu\text{m}$)

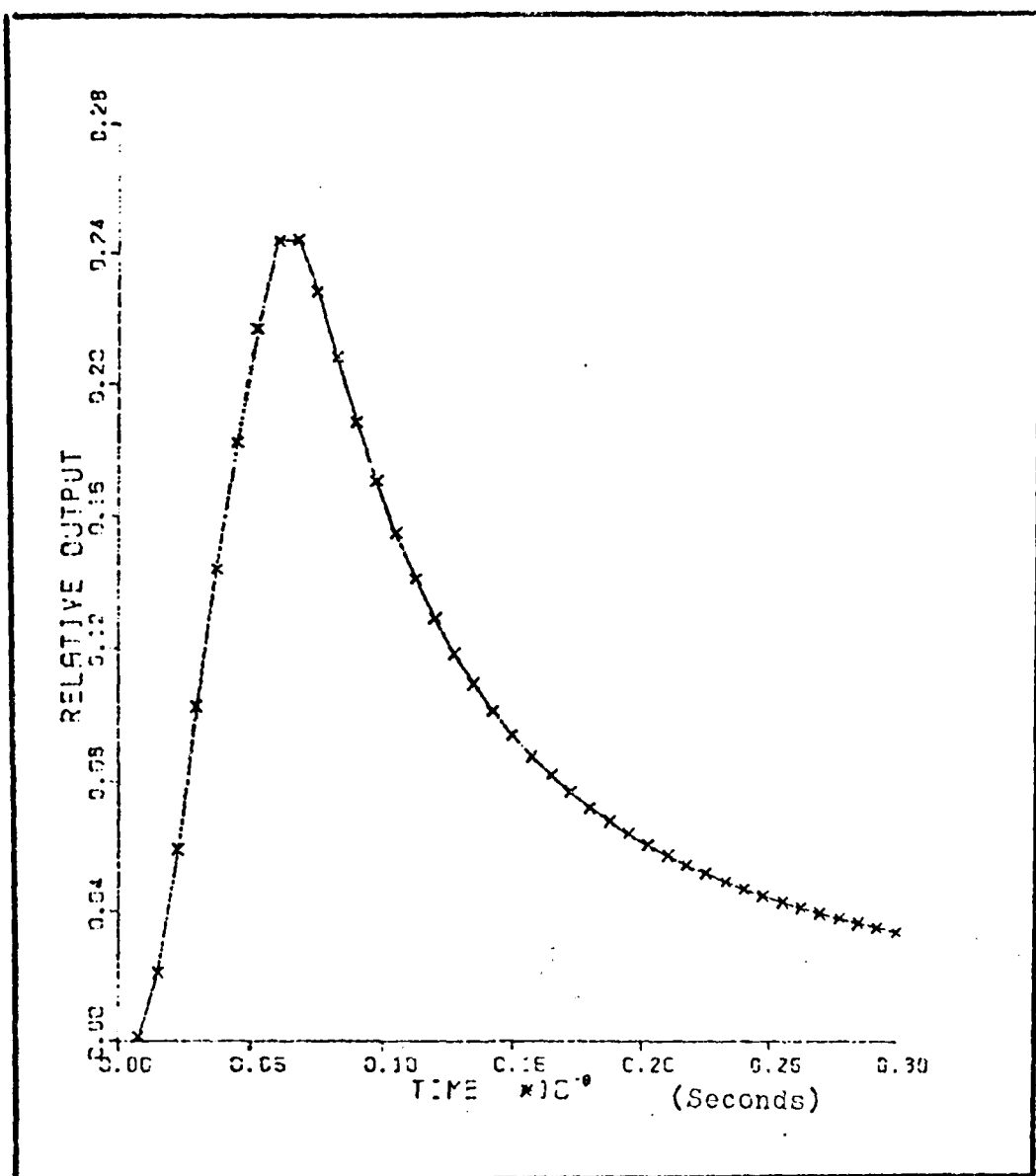


Figure B-11. Computer Plot (D=100, L=4um)

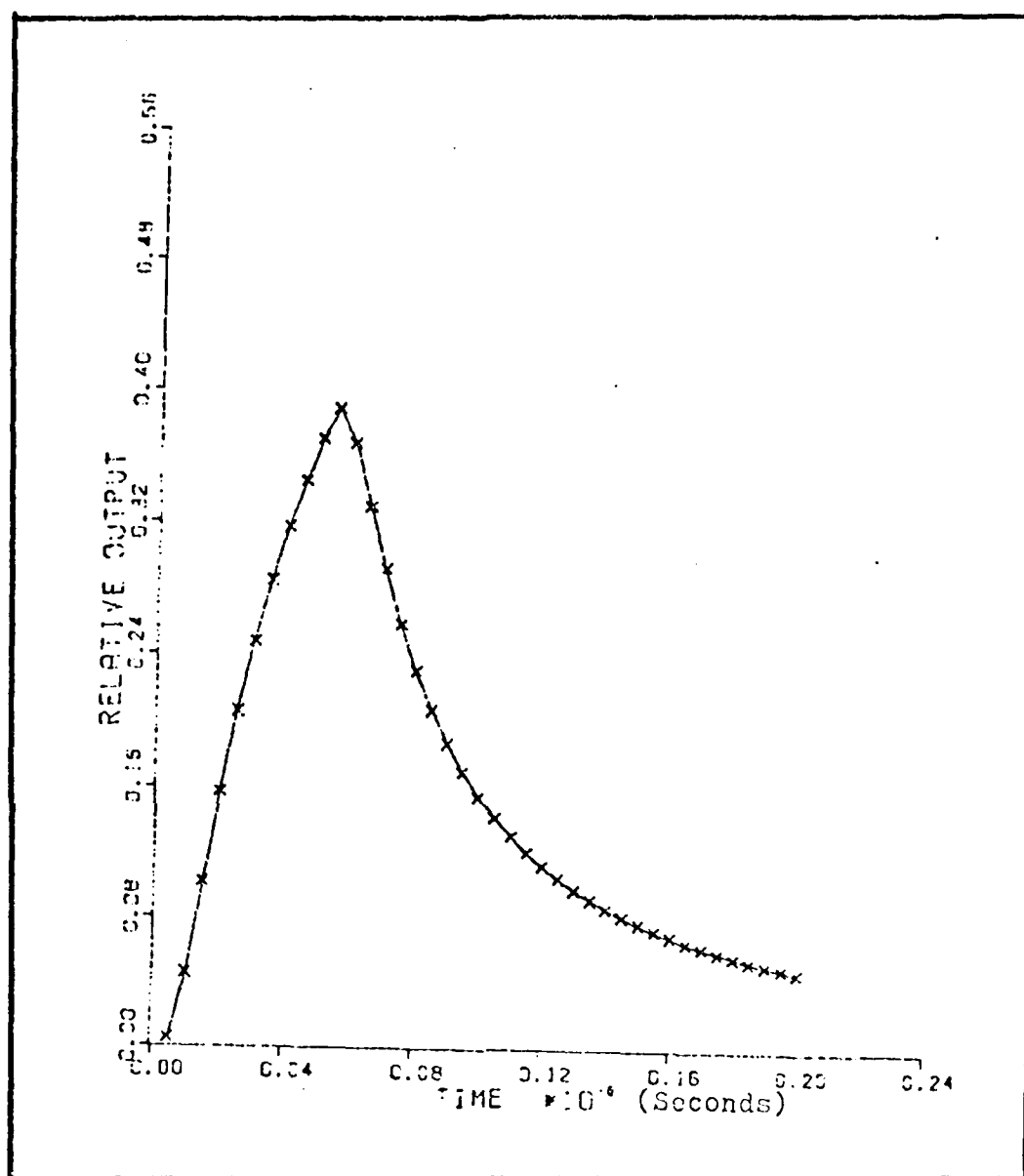


Figure B-12. Computer Plot ($D=200$, $L=4\mu m$)

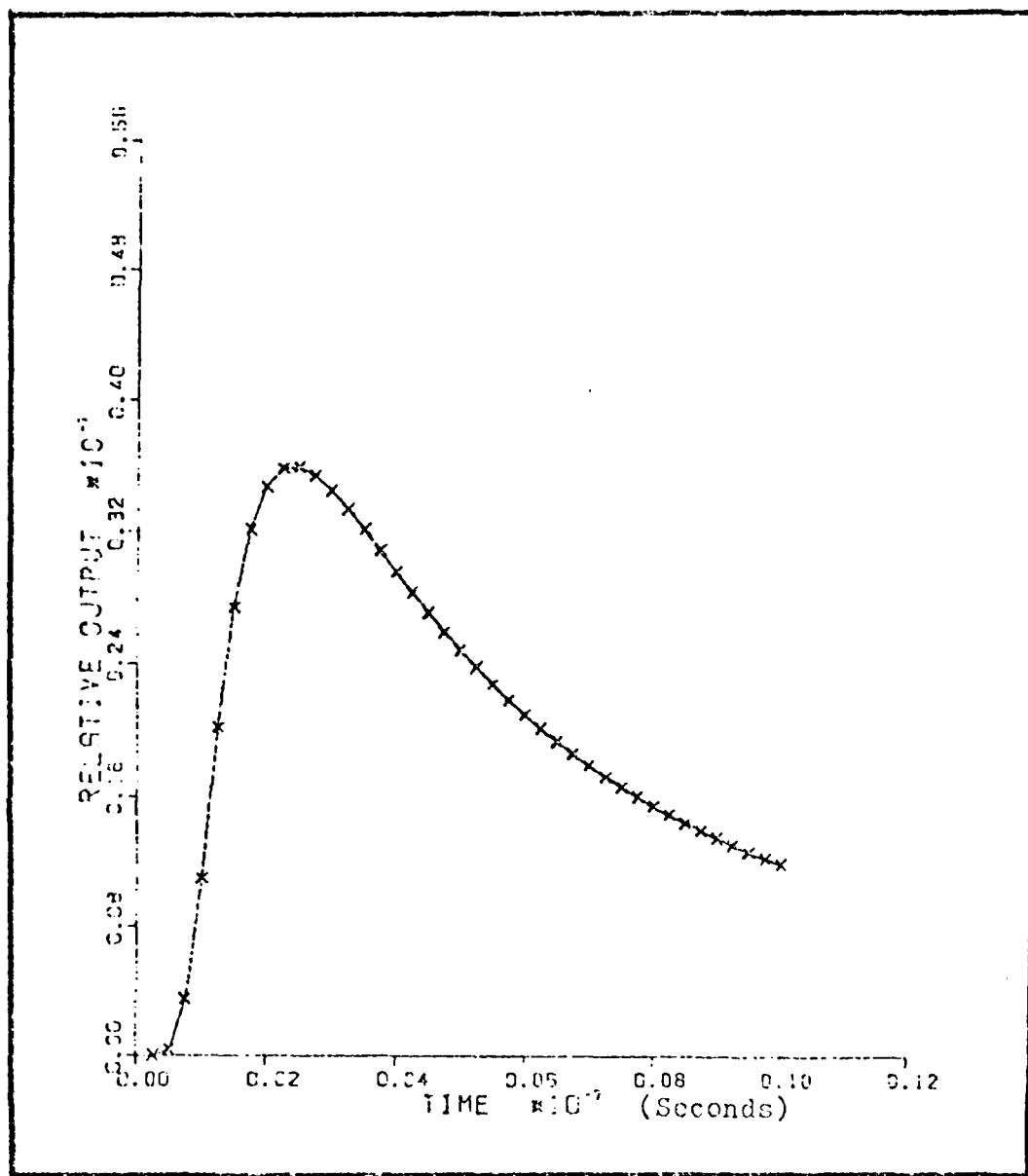


Figure B-13. Computer Plot (D=50, L=8um)

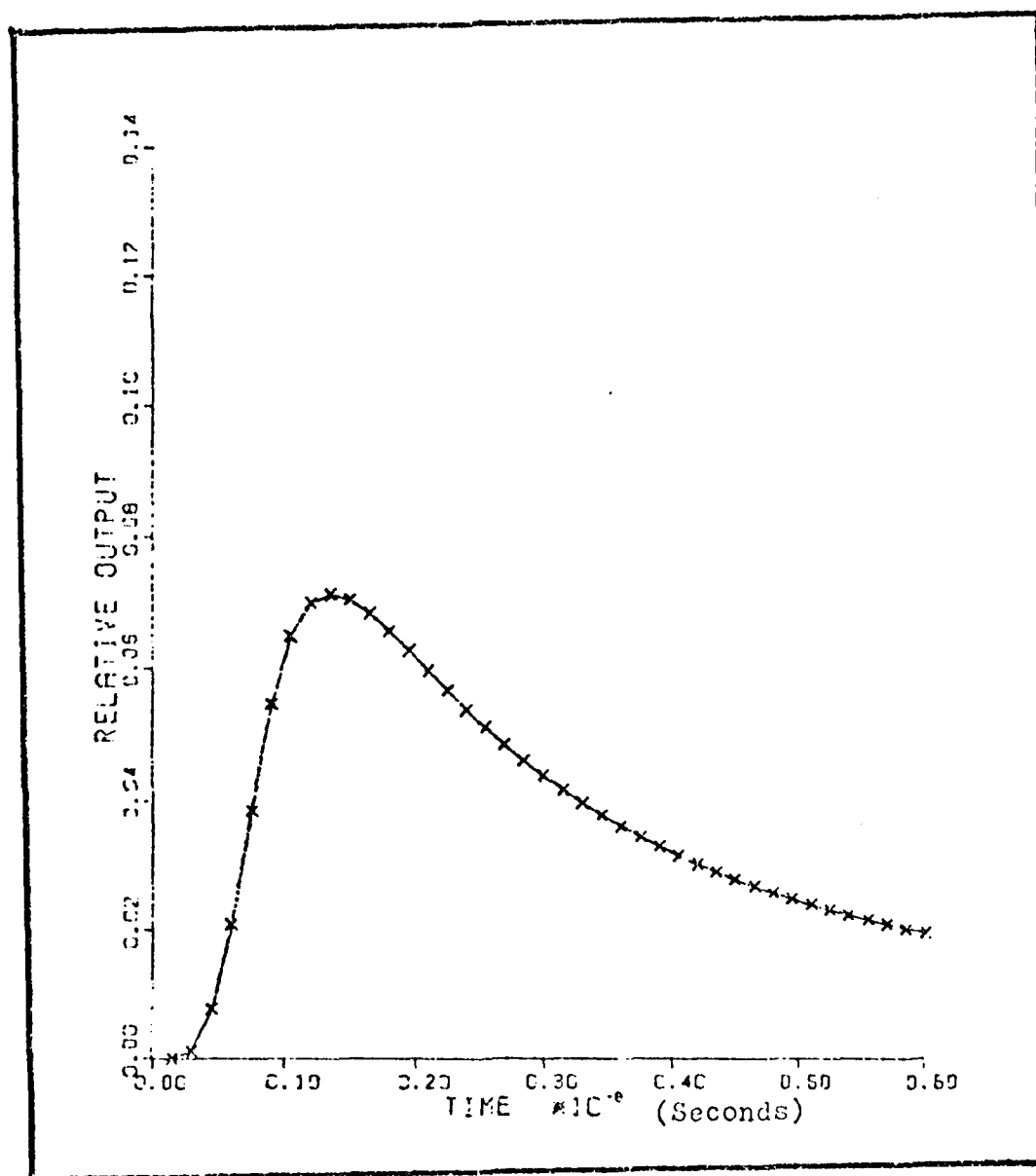


Figure B-14. Computer Plot (D=100, L=8um)

Appendix C

Filter/Spectrometer Calibration

RG-715 Filter

The RG-715 transmission characteristics were measured using a Perkin-Elmer Model 350 Spectrophotometer located at AFIT. The plot of this response is shown in Figure C-1.

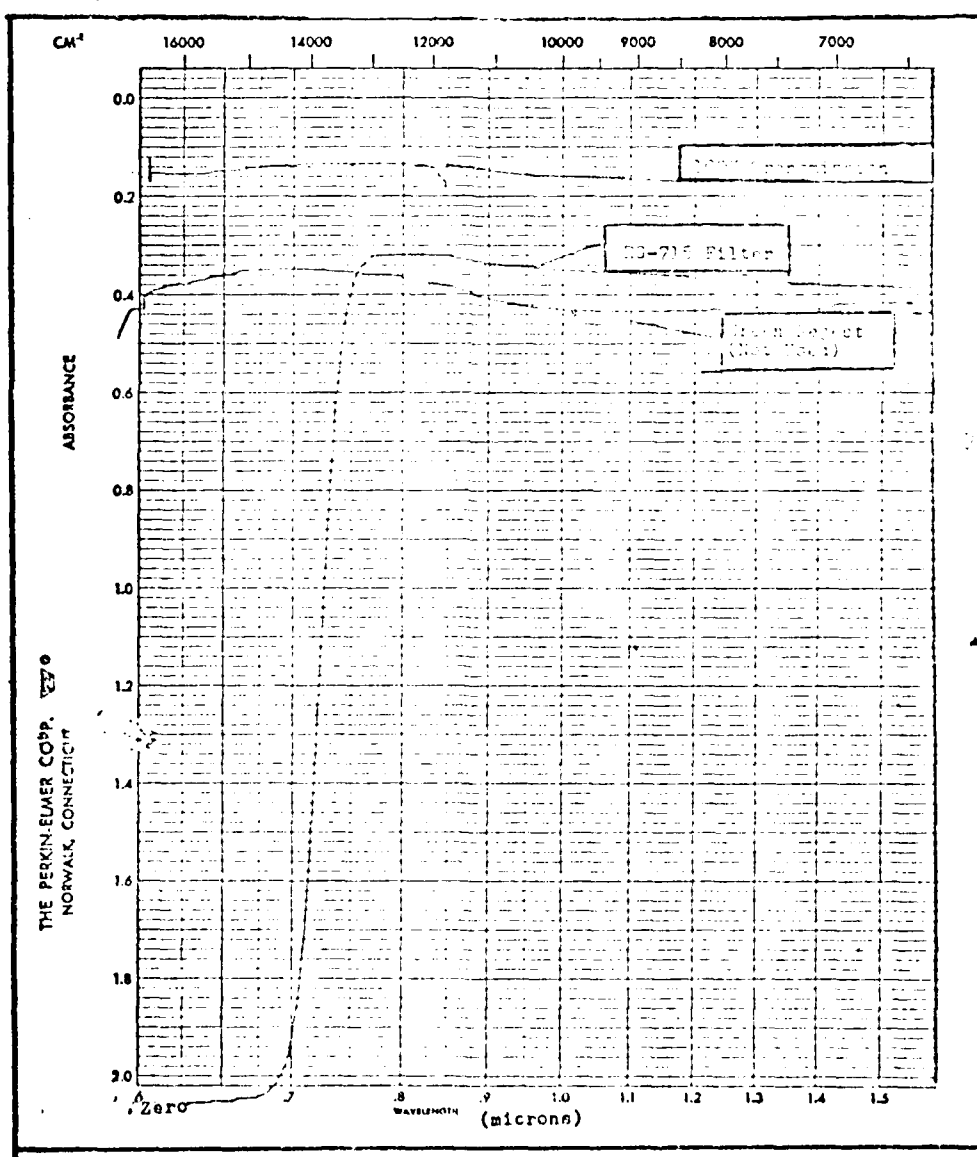


Figure C-1. RG-715 Filter Response

Spectrometer

The Jobin Yvon Model 5/392 UV spectrometer was calibrated using the spectral lines of various sources. The RG-715 filter was placed in front of the spectrometer to eliminate second order lines resulting from spectral lines below 750 nanometers. The following spectral lamp types were tested:

Cs, Ar, Ne, HgNe, Rb, K, Kr

The various lines shown on the chart recorder were compared to spectral lines in the CRC Handbook. A number of spectrums are reproduced in Figures C-2 & C-3 with spectral lines from the handbook indicated. The spectrometer is judged accurate to within 0.5 nanometer.

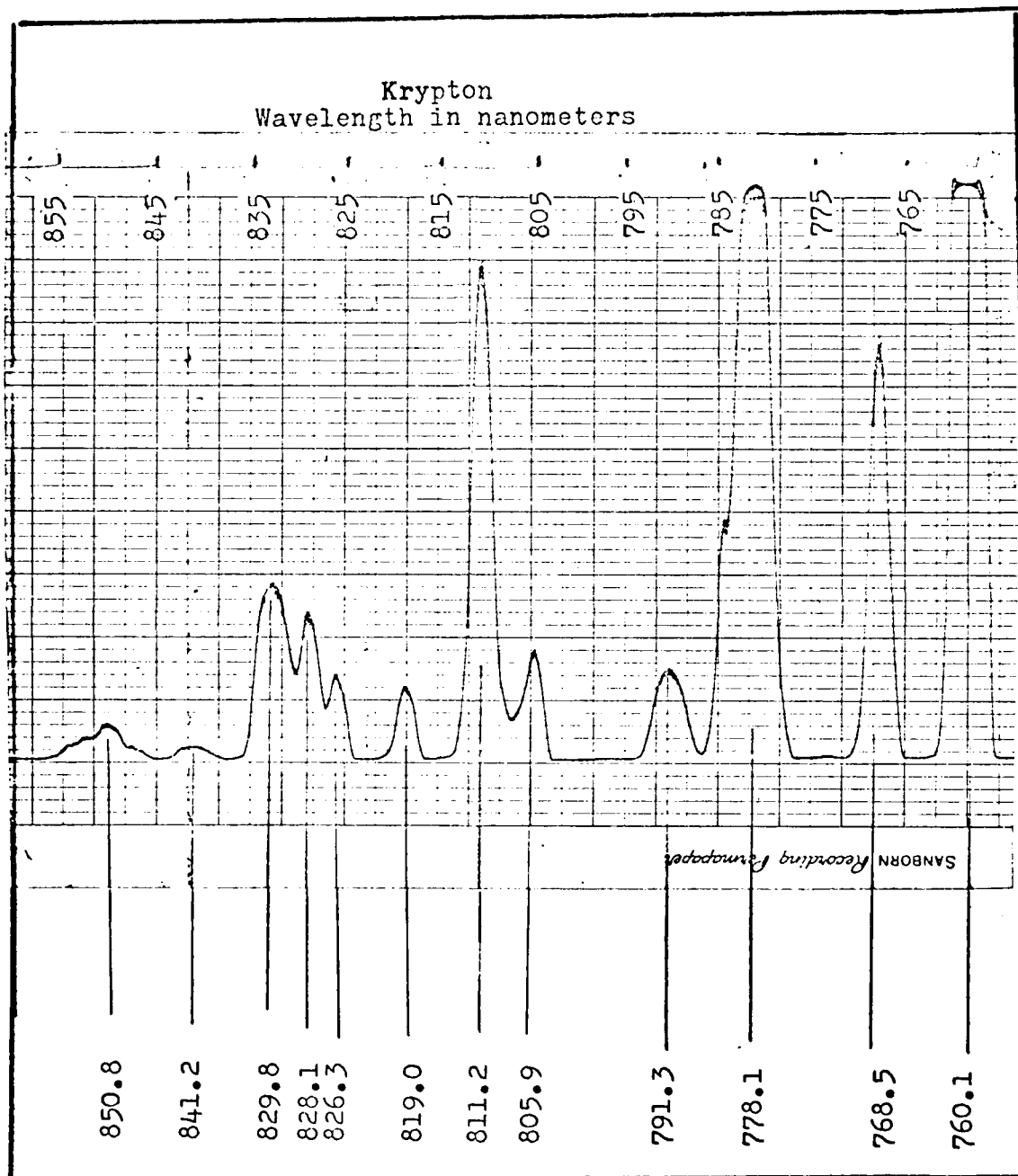


Figure C-2. Krypton Spectrum

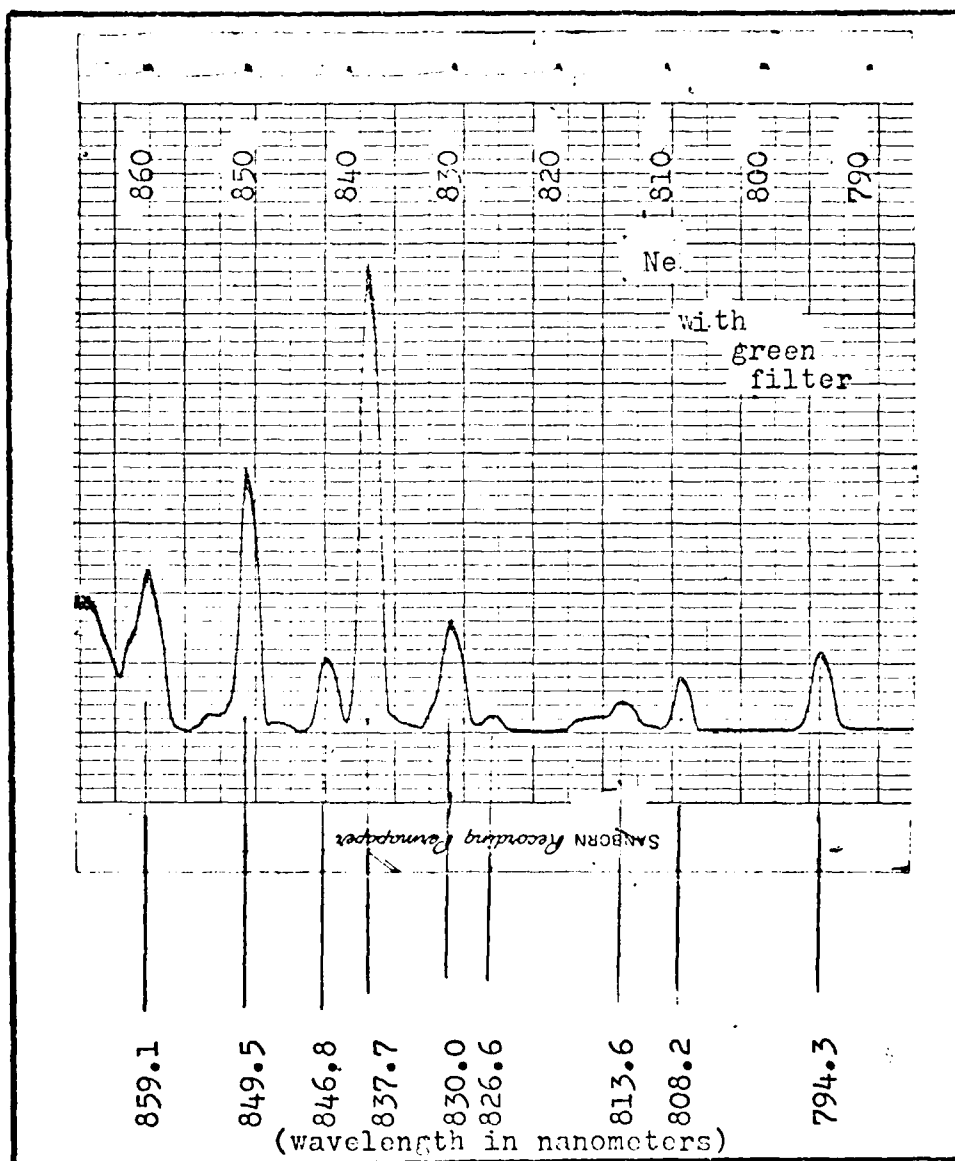


Figure C-3. Neon Spectrum

Spectrometer/Photomultiplier Combination

The Jobin Yvon spectrometer was used in conjunction with an ITT F4102 photomultiplier or an FMI Type 9816 photomultiplier. The response of the photomultiplier cathode material is important in calculations of relative intensity of spectral components. A laboratory standard tungsten lamp whose output intensity profile is shown in Figure C-4 was used to excite the spectrometer/photo-multiplier combination.

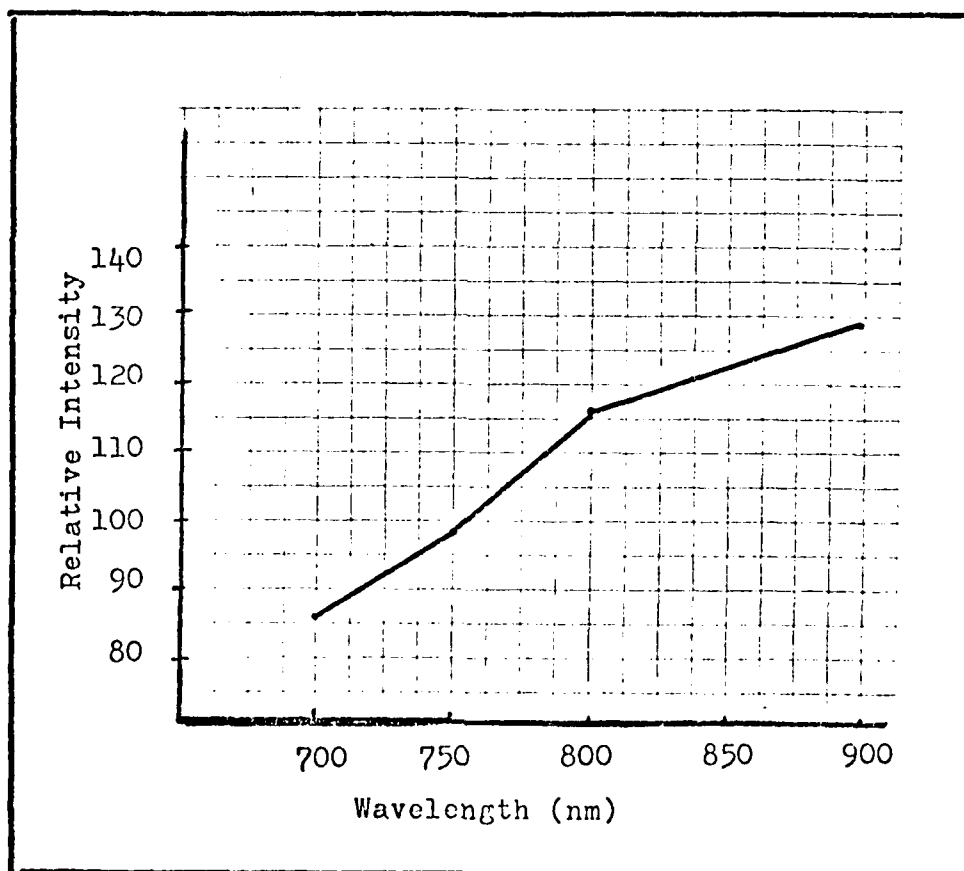


Figure C-4. Intensity Profile of Standard Lamp

The RG-715 filter was placed in front of the spectrometer to simulate the typical experimental configuration. The experimental set-up is shown in Figure C-5 below.

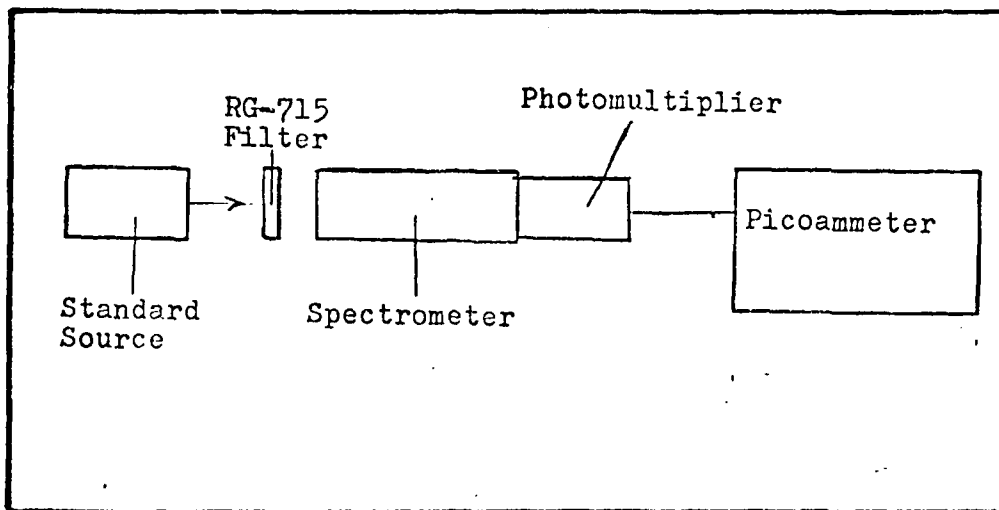


Figure C-5 Spectrometer/Photomultiplier Calibration Set-up

A picoammeter was used to record intensity levels. The spectrum was scanned manually and measurements taken. The levels recorded were normalized by the intensity profile from Figure C-4 and the results presented in Figure C-6 for the ITT tube and Figure C-7 for the EMI tube. It is apparent that the ITT tube contains an extended S-20 response in comparison to the EMI tube. Notice both tubes have a relative peak at 800 nanometers roughly 2.5 to 3.5 times higher than at 820 nanometers. An overlay of both response curves is shown in Figure C-8.

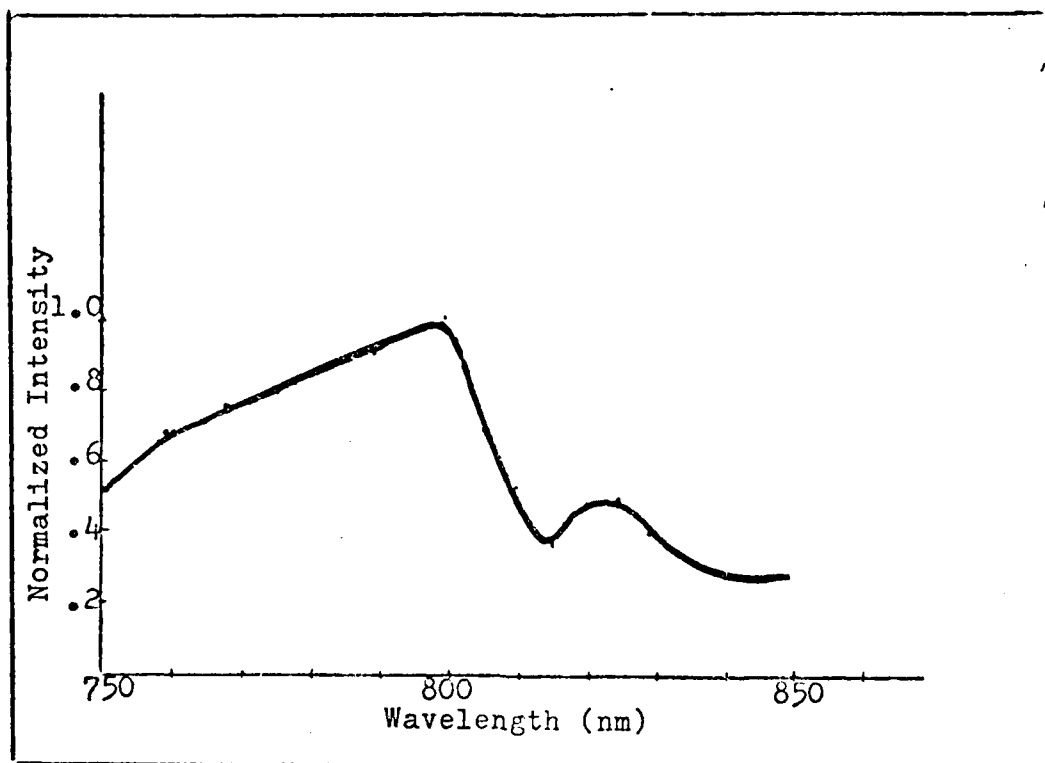


Figure C-6. ITT Photomultiplier Response

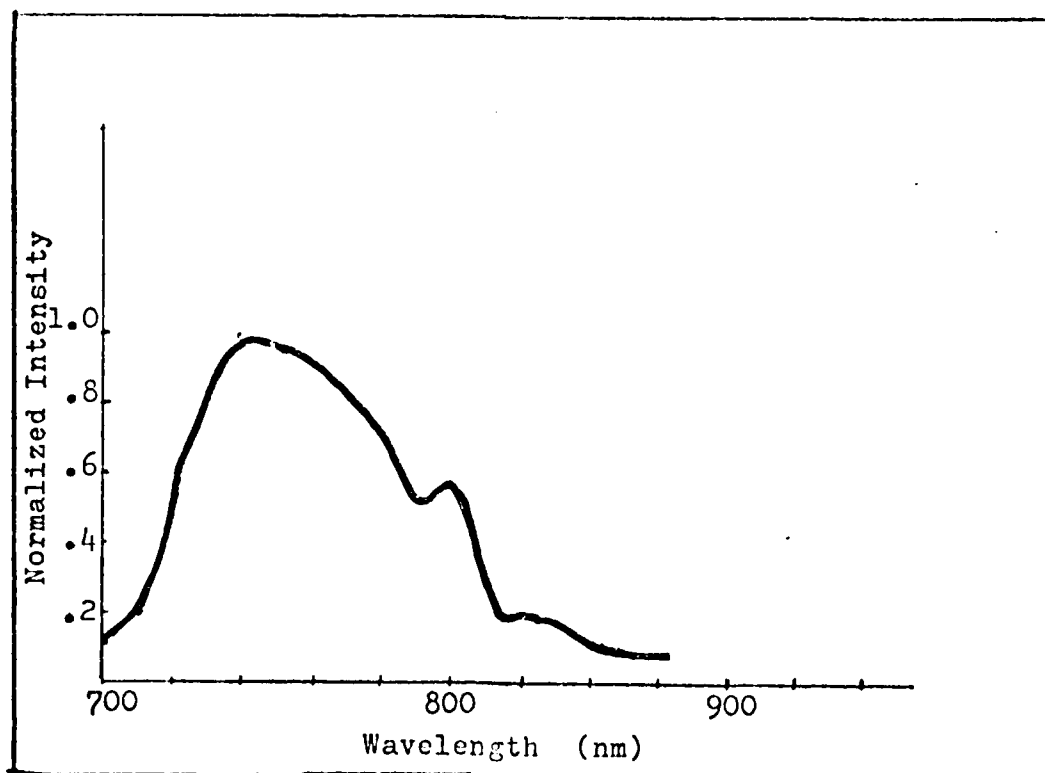


Figure C-7. EMI Photomultiplier Response

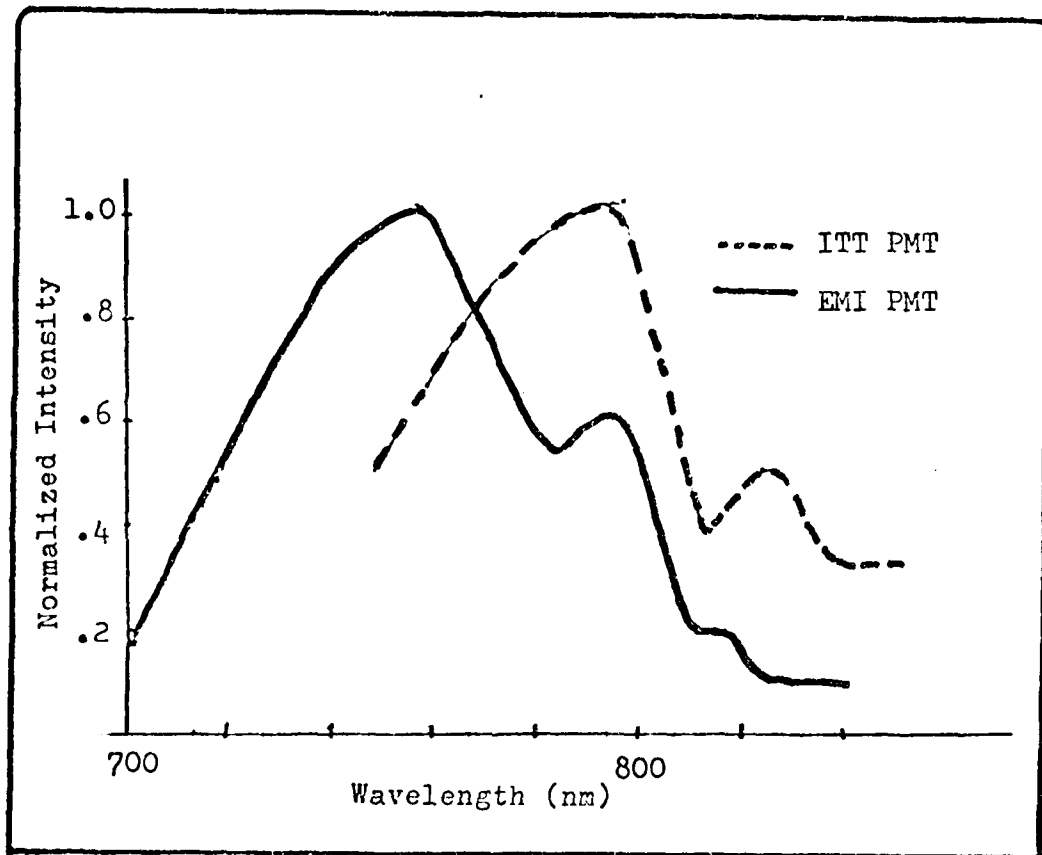


Figure C-8. Comparison Of ITT/EMI Photomultiplier Response

Appendix D

Scattering Experiment

In order to eliminate scattering as a possible source of higher than band gap excitation, an experiment to measure the scatter of the spectrometer was conducted. The experimental configuration is shown in Figure D-1 below.

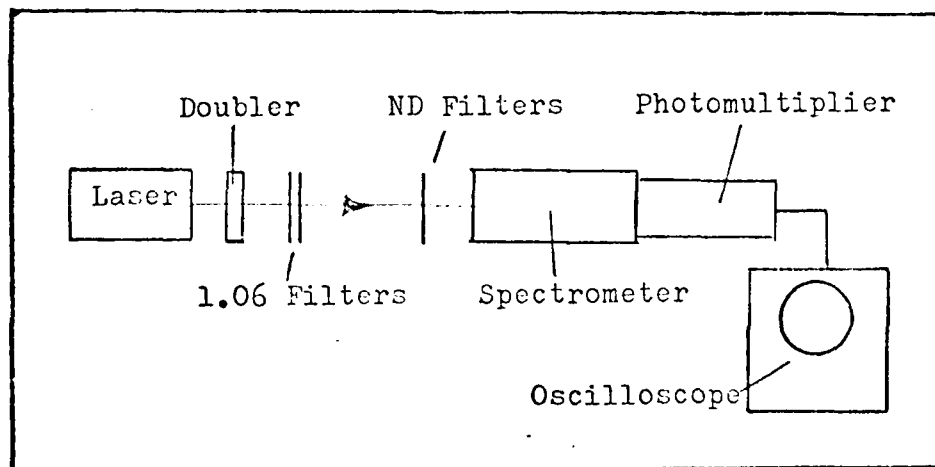


Figure D-1. Scatter Experiment Schematic

The spectrometer was illuminated with the laser. Note that the laser contains both a 532 and 556 nanometer line. The spectrometer was scanned from 530 nanometer to 800 nanometers and the amplitude read off the oscilloscope display. Various neutral density filters were used to attenuate the beam. The data taken are shown in Table II. The intensity was normalized and a plot on logarithmic paper is shown in Figure D-2.

It is evident that scatter is negligible.

Table II

Scatter Measurement Data

Wavelength (nanometers)	Scope Reading (mv)	Filter (OD)	Magnitude (Normalized)	Scatter (%)
800	15	---	0.0000075	0.00075
700	20	---	.00001	.001
600	40	---	.00002	.002
570	100	---	.00005	.005
560	400	---	.0002	.02
553	2000	3.0	1.0	---
540	250	0.6	.00049	.049
532	2000	3.0	1.0	---

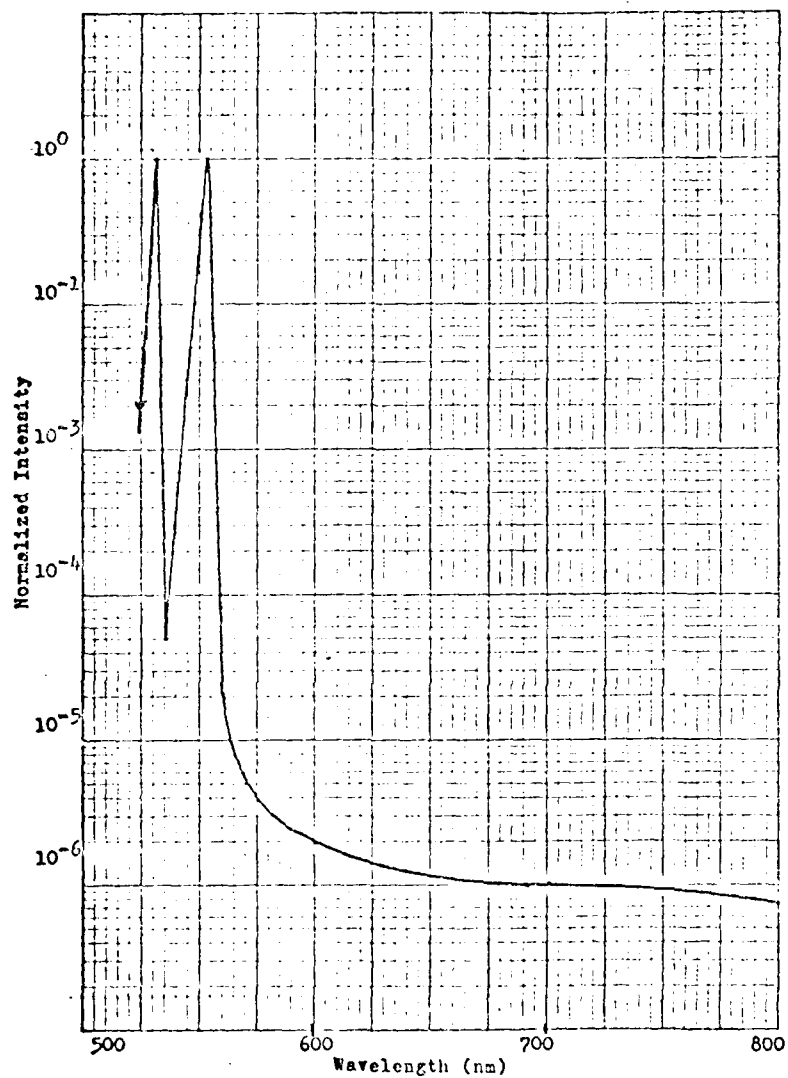


Figure D-2. Scatter Measurement Plot

VITA

Gary Alan Blecker was born 20 May 1952 in Phillipsburg, New Jersey. He graduated from high school in Salem, New Hampshire in 1970 and attended Lowell Technological Institute, Lowell, Massachusetts where he obtained the degree of Bachelor of Science in Electrical Engineering with High Honors in May 1974. He was commissioned through AFROTC into the Air Force in May 1974 and entered active duty in September 1974. He served as a Communications Officer for the 6595 Missile Test Group/Minuteman Division until July 1977 at Vandenberg AFB, California. He then worked for the Deputy for E-4, at Electronic Systems Division, Hanscom AFB, Massachusetts as a test director until entry into the School of Engineering, Air Force Institute of Technology, in June 1977.

Permanent address:

3 Old Derry Rd
Salem, New Hampshire
03079

AD-A094 402

AIR FORCE INST OF TECH WRIGHT-PATTERSON AFB OH SCHOO--ETC F/G 20/12
MEASUREMENT OF THE MINORITY CARRIER DIFFUSION RATE IN N-GAAS.(U)
DEC 80 G A BLEEKER
AFIT/8EO/PH/80-4

NL

UNCLASSIFIED

2 of 2

AL
8/10/80



END

DATE
FILMED

2 81

DTIC

UNCLASSIFIED

SECURITY CLASSIFICATION OF THIS PAGE (When Data Entered)

REPORT DOCUMENTATION PAGE		READ INSTRUCTIONS BEFORE COMPLETING FORM
1. REPORT NUMBER AFIT/GEO/PH/80-4	2. GOVT ACCESSION NO. AD-A094402	3. RECIPIENT'S CATALOG NUMBER
4. TITLE (and Subtitle) MEASUREMENT OF THE MINORITY CARRIER DIFFUSION RATE IN N-GaAs.		5. TYPE OF REPORT & PERIOD COVERED MS Thesis
7. AUTHOR(s) 10 Gary A. Bleeker Captain USAF		6. PERFORMING ORG. REPORT NUMBER
9. PERFORMING ORGANIZATION NAME AND ADDRESS (AFIT-EN) Air Force Institute of Technology Wright-Patterson AFB, Ohio 45433		8. CONTRACT OR GRANT NUMBER(s)
11. CONTROLLING OFFICE NAME AND ADDRESS		10. PROGRAM ELEMENT, PROJECT, TASK AREA & WORK UNIT NUMBERS
14. MONITORING AGENCY NAME & ADDRESS (if different from Controlling Office) (12) 98		12. REPORT DATE Dec 1980
		13. NUMBER OF PAGES 85
		15. SECURITY CLASS. (of this report) Unclassified
		15a. DECLASSIFICATION/DOWNGRADING SCHEDULE
16. DISTRIBUTION STATEMENT (of this Report) Approved for public release; distribution unlimited		
17. DISTRIBUTION STATEMENT (of the abstract entered in Block 20, if different from Report) Approved for public release; IAW 190-17 06 JAN 1981 : Frederick C. Lynch, Major, USAF Director of Public Affairs		
18. SUPPLEMENTARY NOTES		
19. KEY WORDS (Continue on reverse side if necessary and identify by block number) Diffusion Rate Exciton Luminescence		
20. ABSTRACT (Continue on reverse side if necessary and identify by block number) A new experimental procedure was developed to directly measure the minority carrier diffusion rate in n-GaAs. A Q-switched Nd-YAG laser was used to excite the sample and the delay between laser excitation and subsequent luminescence of the sample was used to determine the diffusion rate. A mathematical model of carrier diffusion was developed and computer plots generated to predict → next page		

DD FORM 1 JAN 73 1473 EDITION OF 1 NOV 65 IS OBSOLETE

012225
SECURITY CLASSIFICATION OF THIS PAGE (When Data Entered)

and analyze the experimental data. With the 4 micron thick sample used, the procedure enabled the researcher to obtain an upper bound in delay time of 350 picoseconds and an approximate diffusion coefficient of 100 cm^2/sec . The spectral components of the luminescence and relative conversion were studied. The luminescent spectra exhibited yet unidentified lines above the band gap energy in addition to the usual set of exciton lines. The conversion efficiency of the laser excitation to photoluminescence was 0.14%.

58 m

